Biomechanical behaviour of lizard osteoderms and skin under external loading

Kéver Loïc[1,*], Damien Olivier[2,3], Arsalan Marghoub[4], Susan E. Evans[5], Matthew K. Vickaryous[6], Mehran Moazen[4], Anthony Herrel[1]

[1]Muséum National d'Histoire Naturelle, Paris, France
[2]Departamento Académico de Ciencias Marinas y Costeras, Universidad Autónoma de Baja California Sur, La Paz, Baja California Sur, México
[3]Consejo Nacional de Ciencia y Tecnología, Ciudad de México, México
[4]Department of Mechanical Engineering, University College London, London, UK
[5]Centre for Integrative Anatomy, Department of Cell and Developmental Biology, University College London, London, UK
[6]Department of Biomedical Sciences, University of Guelph, Guelph, ON, Canada

[*]Corresponding author: loickever@gmail.com (ORCID: 0000-0003-3672-5348)

Keywords: Bone-Functional morphology-Squamata-Osteoderms-Stiffness-Strain gauges

Summary statement

We compared biomechanical properties of temporal osteoderms in eleven lizard species and found significant differences in stiffness between taxa reflecting differences in micro- and macrostructure and, likely, in function.

Abstract

Many species of lizards are partially enveloped by a dermal armour made of ossified units called osteoderms. Lizard osteoderms demonstrate considerable species-specific variation in morphology and histology. Although a physical/protective role (against predators, prey, conspecifics, and impact loading during falls) is frequently advanced, empirical data on the biomechanics of lizard osteoderms are scarce, limiting our understanding of form-function relationships. Here, we report deformation recorded at the surface of temporal osteoderms

during controlled external loading of preserved specimens of eleven lizard species (*Tiliqua rugosa, Tiliqua scincoides, Corucia zebrata, Pseudopus apodus, Timon lepidus, Matobosaurus validus, Broadleysaurus major, Tribolonotus gracilis, Tribolonotus novaeguineae, Heloderma horridum* and *Heloderma suspectum*). Based on the strains recorded *in situ* and from isolated osteoderms, the skin of the species investigated can be ranked along a marked stiffness gradient that mostly reflects the features of the osteoderms. Some species like *Tiliqua rugosa* and the two *Heloderma* species had very stiff osteoderms and skin while others like *Timon lepidus* and *Pseudopus apodus* were at the other end of the spectrum. Histological sections of the osteoderms suggest that fused (vs. compound) osteoderms with a thick layer of capping tissue are found in species with a stiff skin. In most cases, loading neighbouring osteoderms induced large strains in the instrumented osteoderm attesting that, in most species, lizard osteoderms are tightly interconnected. These data empirically confirm that the morphological diversity observed in lizard osteoderms is matched by variability in biomechanical properties.

Introduction

Animals can be subjected to traumatic events that damage their tissues, sometimes with lethal consequences (e.g. Jennings, 2009; Tanke and Currie, 1998; Thomas and Cole, 1996). Physical stresses are generated in biological tissues when an individual impacts the ground or objects in its environment, but damage may also occur under the action of an opponent's or predator's claws, teeth, beaks, tails, hoofs, or horns, for example (e.g. Mukherjee and Heithaus, 2013; Song et al., 2011). As such strong loading regimes likely induce different patterns of loading, one could hypothesize that they likely create a wide range of species-specific selective pressures and, consequently, may have promoted the diversity of protective structures that have evolved in animals (see also Connors et al., 2019). For example, loading during agonistic interactions and falls likely constrained the cranial design of primates (e.g. Carrier and Morgan, 2014; Hylander and Johnson, 1997; Hylander et al., 1991).

A potential shielding strategy against traumatic events involves the incorporation of dermal bony plates also known as osteoderms (Vickaryous and Sire, 2009). Such plates are present in several distantly related vertebrate taxa (Yang et al., 2013), yet are particularly common and diverse among extant lizards (Vickaryous and Sire, 2009; Williams et al., 2021). Osteoderms with various shapes and types of organization have been reported for many lizard families (see Williams et al., 2021 for an

exhaustive list) including scincids (e.g. Canei and Nonclercq, 2020; Oliver, 1951), lacertids (Arnold, 1973; Arnold, 1989), gekkonids (e.g. Laver et al., 2020; Paluh et al., 2017), anguids (e.g. Strahm and Schwartz, 1977; Zylberberg and Castanet, 1985), gerrhosaurids, and cordylids (e.g. Broeckhoven et al., 2018a; Marques et al., 2019).

Lizard osteoderms have classically been considered to have a protective function against predators (Williams et al., 2021), but this simplistic view has been challenged, notably by results from phylogenetically informed comparative studies on cordylids (Broeckhoven, 2022; Broeckhoven et al., 2018a; Broeckhoven et al., 2018b; Stanley, 2013). Indeed, the covariation between osteoderm expression, distribution or morphology and ecological factors like climate suggests that osteoderms likely have a multi-functional nature including thermoregulation (e.g. Clarac et al., 2019; but see Inacio Veenstra and Broeckhoven, 2022) and mineral storage (Broeckhoven and du Plessis, 2022). To date, our understanding of osteoderm function(s) suffers from a lack of data relating osteoderm structural features and their biomechanical and thermal properties. The sole empirical data available for lizard osteoderms were provided by Broeckhoven *et al.* (2015; 2017) and suggest that the resistance of cordylid skin to predator bites increases with osteoderm thickness. Simulations using single osteoderms reconstructed from high resolution µCT-scans have also been proven insightful (Broeckhoven et al., 2017; Iacoviello et al., 2020), highlighting, for example, how vascularization or material density can impact stress magnitudes and stress distributions. Surprisingly, two simpler yet fundamental questions have never been addressed: Are there interspecific differences in the *in toto* deformation of lizard osteoderms under external loading? Can these differences be quantified? Aside from improving our understanding of osteoderm function and evolution, answers to these questions would also be useful for applied research. Lizard osteoderms are regarded as valuable models for the development of biomimetic materials such as protective clothing (Broeckhoven et al., 2017; Iacoviello et al., 2020; Liang et al., 2021) but are rarely the topic of biomimetic studies. Insights into the biomechanics of the lizard body "armour" and the forces that have driven the evolution of their diversity could provide valuable insights for the bioinspiration of protective materials.

In this study, we measured deformation in morphologically different osteoderms. To do so we instrumented temporal osteoderms of formalin fixed specimens from eleven species of lizards with different osteoderm shapes and distribution patterns (Fig. 1). Next, we applied two loading regimes roughly mimicking either a bite or an impact on different locations of the head. Our goals were to 1) test whether loadings applied at different locations of the head generated strains in the instrumented osteoderm, 2) whether species differed in the relative stiffness of their osteoderms and skin, 3) whether the two loading regimes ("static" versus "dynamic") differed, thus providing

insights into the morphological features and the patterns of organization driving variation in osteoderm stiffness.

Materials and Methods

Sampling

Our experimental setup required specimens with at least one osteoderm that is larger than the smallest strain gauge available. We worked on temporal osteoderms because they are generally larger than the body and tail osteoderms and are not fused with skull bones. Data were collected for 11 species with two to six individuals per species (Table 1). All the specimens were adults that had been formalin-fixed and preserved in 70% ethanol, and are housed at the Muséum National d'Histoire Naturelle in Paris. Small differences in the fixation protocol (*e.g.* time spent in formalin, formalin concentration) cannot be excluded for the specimens from the MNHN collections causing the intraspecific variability to increase.

'*In toto*' experiment

Instrumentation of the target osteoderm

An osteoderm located in the temporal area was instrumented for every specimen (Fig. 2). The epidermis and the periosteum of the target osteoderm were removed with a scalpel and the surface of the osteoderm was cleaned with hydrogen peroxide, allowing the strain gauge to be glued to the external surface of the osteoderm using cyanoacrylate glue.

The smallest model of rectangular rosette strain gauge (item code: MMF402103; gauge total surface:1.33 mm x 2.9 mm; grid resistance: 350 ohms; gauge factors: 1.7-1.9) manufactured by Micro-measurements (Vishay groups, France) was selected for these experiments. The rosette configuration was favoured because it bears three recording units and therefore can provide tensile, compressive and shear strains in every direction of the gauge plane which here corresponds to the external surface of the instrumented osteoderm.

Loading of the osteoderms

The target osteoderm was loaded by applying an external force orthogonally to the surface at 14 different locations of the animal head (Figs. 2A and 3A). The loading was applied directly on the

instrumented osteoderm (when the osteoderm surface was not entirely covered by the gauge), on several neighbouring osteoderms, and to the rostral area. First, the force was applied for a very short period of time (< 0.1 s, Fig. 2B) using a piezoelectric hammer (Model 086E80, PCB Piezotronics S.A., Saint Aubin, France). As the force-time slope was very steep, we refer to this loading regime as "dynamic" loading. Second, force was applied slowly and for a relatively long period of time (>0.5 s, Fig. 2B) using a metal pin mounted on a Kistler piezo-sensor. The signal generated by the piezo-electric sensor and amplified by a 5011B charge amplifier (Kistler Instrumente AG,Winterthour, Switzerland) provided the magnitude of the load. Since the force was gently increased by hand, we will refer to this experimental set-up as the "static" loading condition hereafter. For each loading location, the procedure was repeated on average 33 times for the "static" loading and 104 times for the "dynamic" loading. More data points were collected during the "dynamic" loading because of the apparent lower consistency in the recording of the force magnitude. In both cases, care was taken to administer forces across the widest possible range of magnitudes (0.01-36.5 N for the "static" loading and 0.01-5.3 N for the "dynamic" loading).

'Tensile test' experiment

Strains recorded *in toto* may not only reflect interspecific differences in the features of the osteoderms themselves. Indeed, the distribution of stresses between osteoderms may be dependent on the thickness and nature of the tissues underlying the osteoderms. Therefore, we tested whether similar trends could be observed in an experimental setup with fewer confounding factors. Six specimens (two *P. apodus*, one *H. horridum*, one *H. suspectum*, two *T. scincoides*, two *T. rugosa* and two *C. zebrata*) with at least one temporal osteoderm that was large enough to drill small holes on its rostral and caudal ends (see 2.3.2) were selected for this experiment. In each case, temporal osteoderms of one side of the head were dissected out and the largest osteoderm was cleaned of any underlying soft tissue and instrumented. Note that, because of the destructive nature of dissections, several specimens from the MNHN collections that are listed in Table 1 were not included in the sampling for this experiment.

Next, two single element gauges (item code: MMF402183; gauge total surface:2.41 mm x 2.6 mm; 350 ohms; gauge factor:1.9) manufactured by Micro-measurements were glued to the dissected osteoderm, one on its external side and the other on its internal side. Single gauges can only provide compressive, tensile, and shear strain along their long axis; here the anteroposterior axis of the osteoderm. They were, however, appropriate considering the goal of this second set of experiments and the loading applied to the osteoderms.

Two small holes (0.8 mm) were drilled through the osteoderms. They were located along the anteroposterior axis of the osteoderm near the edges. One of these holes was used to hang the osteoderm from a stand (Fig. 2). The second hole was used to load the osteoderm with a series of weights (100g, 200g, 500g, and 700g) using a thin wire. Consequently, the force vector resulting from the weight and the long axis of the gauge were aligned. The force applied to the osteoderm was obtained by multiplying the mass by the gravitational acceleration (F=m*g). In a second experimental setup, the osteoderm was held horizontally using forceps and the weight vector was oriented perpendicular to the anteroposterior axis of the osteoderm (Fig. S1). This experiment was conducted on an even smaller sample of individuals because some osteoderms were too small to be held using forceps.

The instrumented osteoderms were prepared following the polishing protocol reported by Marghoub *et al.* (2022) and sectioned along the axis of the force vector in a way that ensured the drilled holes were in view. Sections performed at the level of the gauges were imaged using a KEYENCE Vhx 7000 Digital Microscope to illustrate the thickness and shape of the osteoderms, the multi-partite morphology of compound osteoderms (characteristic of some skink species), and to document the presence and proportion of capping tissue (*i.e.* osteodermine) described by Marghoub *et al.* (2022) and Kirby *et al.* (2020).

Strain recording and analysis

The gauges were connected with a 2310 signal conditioning amplifier (Vishay, Malvern (PA), U.S.A) set up to feed the gauges with a 1.4 V current. Changes in the resistance of the gauges caused by changes in the gauge length resulted in voltage variations that were captured and amplified by the differential amplifier. The output signals from the amplifier were then converted from analog to digital and synchronized in a MP150 data acquisition and analysis system (BIOPAC System Inc., Goleta (CA), USA). For the *in toto* experiment, the force signal recorded from the piezoelectric sensors was synchronized with the recordings of the strain using the MP150. The output of the BIOPAC was recorded on a laptop in the Acknowledge 4 software (BIOPAC).

Using calibration data and a series of “homemade” Igor (Wavemetrics, Inc., Portland (OR), USA) procedures, the force and strain signals were calibrated, transformed and analysed. For strains recorded from the rectangular rosette gauges (experiment 1), the data recorded from each element of the gauge were used to calculate the maximal principal strain (maximal tensile strain in the plane of the gauge), the minimal principal strain (maximal compressive strain in the plane of the gauge), the Shear strain (maximal-minimal principal strain), and the angle between the element A of the

gauge and the maximal principal strain. The procedure used for the analysis first located the peaks of force then measured the maximal force and the largest strain associated with each peak. Strain values recorded from the 'Tensile test' experiment were measured manually in the 'AcqKnowledge' software. Here, the compressive and tensile strains caused by the attached weight were recorded as soon as the signal became stable.

Statistical analysis

We ran Linear Mixed Models (LMMs) using the maximal tensile and compressive strains recorded at the level of the outer surface of the instrumented osteoderm and the following covariates: loading force, loading location, species, specimen, and specimen head length. For each of the next four hypotheses, several models were run in R (2016) with the *lmer* function of the lme4 package (Bates et al., 2018).

1) *For a given loading force, the largest strains are always measured when the loading was applied directly on the instrumented osteoderm (vs. other locations in the head)*. Here, we considered the covariates 'Location', 'Loading force', and their interaction as fixed factors and the covariates 'Species', 'Specimen', and 'Head Length' as random effects. The interaction between 'Specimen' and 'Location' was also considered as a random effect to deal with the pseudo-replications.
2) *There are interspecific differences in the stiffness of the 'skin system' (i.e. osteoderm and soft tissues of the skin)*. Here, the covariates 'Species', 'Loading' force, and their interactions were considered a fixed factor while the other covariates were modelled as random effects.

For the purpose of testing hypotheses 3 and 4, a variable 'Group' was added to the dataset. This 'Group' variable had four different levels: (0) loadings at the rostral end of the head (Fig. 3A, 11-14), (1) loadings on osteoderms that are separated from the instrumented osteoderm by one osteoderm (Fig. 3A, 8-10), (2) loadings on osteoderms that are adjacent to the instrumented osteoderm (Fig. 3A, 4-7), and (3) loadings on the instrumented osteoderm (Fig. 3A, 1-3). *Matobosaurus validus* specimens were excluded from these models because we were not able to load the instrumented osteoderm directly (*i.e.* gauges occupied most of the osteoderm surface).

3) *There are interspecific differences in the stiffness of osteoderms.* Here, we focused on strains measured for loading locations that are on the instrumented osteoderm (Group 3) to exclude the effects of factors like stress transmission between osteoderms and skull morphology, for example. The data obtained from the 'Tensile test' experiment were also used to test Hypothesis 3.

4) *There are interspecific differences in the transmission of the force between neighbouring osteoderms.* Here we investigated relative differences in strains predicted for groups 0, 1, 2, and 3 within each species to determine which species transmit more force from the loading location to the instrumented osteoderm. For each model, the compressive and tensile strain predicted (using the median loading forces) for each combination of species and group were normalized between 0 and 1. This was achieved by dividing the strain values predicted for each combination of species and group by the highest values predicted for a group of the same species. These data provide a sense of the relative changes in the strains recorded in the instrumented osteoderm when the same loading force was move moved from group 3 to 0. The underlying idea is that in some species the strains could decrease by small increments (*e.g.* 100% of the strain when the instrumented osteoderm is loaded directly, 90% when the adjacent osteoderms are loaded, and 70% when the osteoderms separated from the instrumented osteoderm by one osteoderm are loaded) while in some other species they would be very large (*e.g.* 100%, 50%, and 10% respectively).

The following equations were used to generate the models:

Hypothesis 1: (STRAIN) ~ (Loading_Force)*Locations+(1|Specimens)+
(1| Specimens:Locations)+(1|Species)+(1|HeadLength)

Hypothesis 2:(STRAIN) ~ (Loading_Force)*Species+(1|Specimens)+
(1| Specimens:Locations)+(1|Locations)+(1|HeadLength)

Hypothesis 3 & 4:(STRAIN) ~ (Loading_Force)* Species * Group+(1|Specimens)+
(1|Specimens:Locations)+(1|Locations)+(1|HeadLength),

where strain refers to tensile and compressive strains in static or dynamic manipulations.

The strain and loading force were log-transformed to fit a normal distribution of the residuals. The visual inspection of the model residuals did not reveal strong violations of parametric conditions (normality and homogeneity of variances). Small to moderate residuals correlations were still observed (from 0.2 to 0.4), which should not affect our interpretation of the models. We performed type III ANOVAs to check whether the fixed effects and their interactions had significant impacts on the measured strains. Next, we used the models to predict the strain under a unique value of loading force. We chose the median applied force value observed in both the static and dynamic loading experiment.

Results

Hypothesis 1: the largest strains are always measured when the loading is applied directly on the instrumented osteoderm

Loading force and loading location significantly impacted the maximal tensile and compressive strains in both the 'static' and 'dynamic' models (Table S1A; $P< 0.0001$). Compressive strains predicted for the 'Static' and 'Dynamic' data tend to confirm our hypothesis that loading of the instrumented osteoderm induced the largest strains recorded at the outer surface of this structure (Triangles in Fig. 3B2 and C2). However, loading of the adjacent osteoderms (Diamonds in Fig. 3 B2 and C2) can also generate large compressive strains in the instrumented osteoderm. This was mostly true when the osteoderm located at the ventral rim of the instrumented osteoderm (Fig 3 B2 and C1, diamond 4) was loaded.

The highest tensile strain in the 'Dynamic' model was predicted for a loading on the instrumented osteoderm (Fig. 3 B1). However, tensile strains with similar magnitude were predicted for loadings on the osteoderm located at the ventral rim of the instrumented osteoderm (Fig. 3 B1, diamond 4). Considering the 'Static' data, the model even predicts greater tensile strains when the loading is applied on adjacent osteoderms (diamond in Fig. 3 C1) instead of the instrumented osteoderm (triangles in Fig. 3 C1).

For both the 'Dynamic' and the 'Static' loading conditions, the models predict much smaller tensile and compressive strains in the instrumented osteoderm when the loaded osteoderm is separated by at least one osteoderm from the instrumented osteoderm (Fig 3). In the case of a loading at the rostral end of the head, the strains generally barely exceeded the background noise (Fig. 3B and C). It is also worth mentioning that loading osteoderms located ventrally or posteriorly to the instrumented osteoderm generally produce larger strains than loading osteoderms that were located anteriorly or dorsally (see 4 vs 5,6,7 and 8 vs 9 ,10 in Fig 3 B and C).

Our data showed that the largest compressive strains are observed when the instrumented osteoderm is loaded directly even though loading of adjacent osteoderms also generates large compressive strains. Loading of the adjacent osteoderms produced tensile strains that were similar ('Dynamic' data) or even larger ('Static' data) than those observed when the instrumented osteoderm is loaded.

Hypothesis 2: There are interspecific differences in the stiffness of the 'skin + osteoderm system'

The static and dynamic models confirmed interspecific variation in osteoderm strains (Species effect: $P < 0.05$, Table S1B) considering all the loading locations. Species can be placed along a stiffness gradient based on the predicted tensile and compressive strains (Fig. 4). This gradient also becomes apparent when looking at the strains predicted for the groups 1 to 3 (Figs. 5 and 6) and species order is highly similar using the different models (Figs. 4, 5 and 6). The osteoderms of *Tiliqua rugosa* and the two *Heloderma* species were stiffer than those of *Timon lepidus*, *P. apodus*, *Tribolonotus gracilis, Tiliqua scincoides*, and, in some instances, *C. zebrata,* whereas the three-remaining species (*Tribolonotus novaeguineae* and the gerrhosaurids *B. major* and *M. validus*) showed intermediate strain values. Our second hypothesis is confirmed with *T. rugosa* standing out as a species with a very stiff skin system whereas the skin of *T. lepidus, T. gracilis* and *P. apodus* appears the least stiff. However, the question remains as to whether these differences are due to the structure or mechanical behaviour of the osteoderm itself.

Hypothesis 3: There are interspecific differences in the stiffness of osteoderms

The 'Group' variable had a significant effect on the strains in every model (Table S1C). When considered alone, 'Species' did not have a significant effect on strain. However, when considered in combination with 'Loading Force' and/or 'Group' its impact was always significant (Table S1C).

Very similar gradients of species were obtained with the four models (Figs. 5, 6, and 7A and B). With the exception of tensile strains predicted for *H. suspectum* during the static loading (Fig. 7B1), the tensile and compressive strains predicted for the *T. rugosa* and the two *Heloderma* species were always very small. On the other hand, large compressive and tensile strains were predicted for *T. lepidus*, *T. gracilis*, *P. apodus*, and *C. zebrata* (except for tensile strains predicted under a static loading). Intermediate values of strain were predicted for the *B. major*, *T. scincoides* and *T. novaeguineae.* The species order along the stiffness gradients is very similar irrespective of whether all loading locations or direct loading are considered, suggesting that the features of the osteoderms strongly impact the biomechanical proprieties of the skin + osteoderm system.

The strains recorded on the external and internal sides of the dissected osteoderms during the 'Tensile test' experiment were several orders of magnitude (at least with the highest weights) larger in *C. zebrata*, *T. scincoides*, and *P. apodus* than in the two *Heloderma* species or in the *T. rugosa* (Fig. 8). The experimental setup, similar to a classical tensile test, confirmed the trends observed *in toto* even though, in the present case, osteoderms appear more elastic in *C. zebrata* and

T. scincoides than in *P. apodus.* Notably, *Pseudopus apodus* is the only species for which we recorded tensile strains on the external surface of the osteoderm. For the other species, we recorded compressive strains on this side of the osteoderm. This was most likely explained by the more convex shape of their osteoderms (Fig. 8). On the internal side, tensile strains were recorded for every species.

Our third hypothesis is confirmed because there were clear interspecific differences in the strains recorded when the instrumented osteoderm was directly loaded. *Tiliqua rugosa* again stood out as having very stiff osteoderms whereas the temporal osteoderms of *T. lepidus*, *T. gracilis*, *P. apodus* were the least stiff. Based on the 'Tensile test' experiment, osteoderms of *T. scincoides* and *C. zebrata,* in particular, were also less stiff.

Hypothesis 4: There are interspecific differences in the transmission of the force between neighbouring osteoderms

We also took advantage of the results provided by the models described in 3.3 to test our fourth hypothesis. During the 'Dynamic' loading, large proportions of the forces causing tensile strains in the instrumented osteoderm were transferred between the different groups of osteoderms in *Tiliqua rugosa* and *H. horridum* and to some extent in *Timon lepidus*, *Tribolonotus novaeguineae* and *Tiliqua scincoides* (upper half schemes under the hammer shapes in Fig. 9). Forces causing compressive strains (lower half schemes under the hammer shapes in Fig. 9) were transmitted in the two *Heloderma* species and in *T. rugosa.* On the other hand, forces causing tensile and compressive strain were rapidly dissipated between the groups of osteoderms in *Tribolonotus gracilis*, *C. zebrata, P. apodus* and *B. major.*

During the 'Static' loading, the forces causing tensile strain in the instrumented osteoderm seemed high in every species, at least between groups 1 to 3 (upper half schemes under the hand shapes in Fig. 9). There were, however, differences in the transmission of forces causing compressive strains with *H. suspectum*, *H. horridum*, *Tiliqua scincoides*, *P. apodus* and *Timon lepidus* showing high levels of transmissions and the two *Tribolonotus* species, *B. major*, *C. zebrata* and *Tiliqua rugosa* showing much lower levels of force transmission (lower half schemes under the hand shapes in Fig. 9).

In addition to the interspecific differences, some species seemed to show differences in the transmission of the force depending on the type ('Static' vs 'Dynamic') of loading. In *Tiliqua rugosa* more force was transmitted under the 'Dynamic' loading (Fig 9). This was especially striking when

investigating the compressive strains. In *B. major*, *P. apodus*, and *C. zebrata* force transmission seemed larger during the 'static' loading, especially when tensile strains were considered (Figure 9).

Discussion

During the last seven decades, strain gauges have been used extensively to quantify minute length changes in loaded human bones (Grassi and Isaksson, 2015). They have also serve the description of strains in bones of other mammals (e.g. Hylander, 1984; Thomason, 1991; Weijs and De Jongh, 1977) and, more recently, of fish (Markey et al., 2006) and reptiles (Dutel et al., 2021; Metzger et al., 2005; Porro et al., 2013; Porro et al., 2014; Ross et al., 2018; Smith and Hylander, 1985). Here, we used strain gauges to record maximal compressive, tensile and shear strain (shear strains are illustrated in Table S1-2 and Fig. S2-S3) in temporal osteoderms of 11 lizard species. We observed that large strains can be recorded when the instrumented osteoderm is directly loaded but also when force is applied to neighbouring osteoderms. We also recorded large strains on the external and internal side of the dissected osteoderms during the 'Tensile' test. Although it may seem counterintuitive that we recorded compressive strains on the external surface for every species but *P. apodus*, this could be explained by the convex shape of the osteoderms (Fig. 8). A clear species gradient emerged from our analyses. The two helodermatids (*H. suspectum*, *H. horridum*) and the *Tiliqua rugosa* had stiff skin and osteoderms. *Timon lepidus, P. apodus* and *Tribolonotus gracilis* were at the other end of the spectrum, with less stiff skin and osteoderms. The osteoderms of *Tiliqua scincoides* and *C. zebrata* had mechanical features more similar to the latter species and very large strains were recorded for these two species when dissected osteoderm were submitted to a 'tensile' test. The two gerrhosaurids (*B. major* and *M. validus*) and the scincid *Tribolonotus novaeguineae* had temporal osteoderms with an intermediate stiffness.

Morpho-functional inferences

In most cases, the stiffness of the osteoderms appeared related to their overall shape. The relatively elastic osteoderms of *Tiliqua scincoides*, *Timon lepidus*, *P. apodus*, and *C. zebrata* are thin and slightly to markedly elongated along the antero-posterior axis whereas the stiff osteoderms of *Tiliqua rugosa* and the two helodermatids are proportionally thicker and more rounded (Fig. 1A). The osteoderms of the two gerrhosaurids had an intermediate shape and biomechanical properties (Fig. 1A). Among cordylids, thicker osteoderms have been shown to provide a better resistance against puncture during predator bites (Broeckhoven et al., 2015; Broeckhoven et al., 2017). We therefore propose

that thickness, inherent mechanical properties and protection against puncture are correlated, and that the dermal armour of *Tiliqua rugosa* and the *Heloderma* species should better resist puncture.

Focusing on the five scincid species, at least three additional features of the gross morphology of the osteoderms likely explain why *Tiliqua rugosa* and *Tribolonotus novaeguineae* had stiff osteoderms compared with *C. zebrata* and *Tiliqua scincoides*. First, the length of the overlapping section of adjacent osteoderms was longer in *Tiliqua rugosa* compared to all the other species, which may have helped increase the overall stiffness of the skin system (Fig. 1A). Second, the temporal osteoderms of *C. zebrata* and *Tiliqua scincoides* have a compound morphology (Fig. 1A), with each element being composed of several smaller bony pieces (termed osteodermites) sutured together with fibrous connective tissue (Williams et al., 2021). This compound organization likely contributed to a reduction in their overall stiffness. In contrast, the temporal osteoderms of *Tiliqua rugosa* and *Tribolonotus novaeguineae* were consolidated elements without intervening fibrous sutures. Third, the midline keel observed in *Tribolonotus novaeguinae* has previously been suggested to reduce vertical stress, at least in crocodylomorph osteoderms (Clarac et al., 2019)

Unexpectedly, osteoderms from the two *Tribolonotus* species (Fig. 1A) demonstrated different loading properties (we recorded larger strains for *Tribolonotus gracilis* as compared to *Tribolonotus novaeguineae*), despite sharing a similar large size (relative to snout-vent length) and shape (with the develop of a strong, midline keel). Investigating structural features of osteoderms may help explain this discrepancy, as histological composition and structural heterogeneity likely alter resistance to external loads (see: Iacoviello et al., 2020). For example, an enamel-like capping tissue with a high Youngs-Modulus has been reported in the dorsal osteoderms of some lizards (Kirby et al., 2020; Marghoub et al., 2022). The thickness of this tissue varies across species (including *H. suspectum* and *P. apodus*) but was absent from the osteoderms of *Varanus komodoensis.* For the temporal osteoderms, we observed a tissue similar to that capping tissue in every species investigated in the 'Tensile test' experiment although it was much thinner and sparsely distributed in *C. zebrata* (Fig. 8). The variation in osteoderm stiffness observed among these species underscores the need for systematic reporting of the presence, thickness, distribution, and functional properties of this capping tissue. In particular, the morphological and functional diversity of scincid osteoderms stands out as an important target for future evolutionary and biomimetic studies of body armour. The biomechanical and morphological data gathered in our study offer a first glimpse of the knowledge that will be gained and the features that could be mimicked to improve the stiffness or elasticity of materials used in the production of armour, vehicles, or helmets, for example.

Using a drop weight impact test on biomimetically manufactured skin sheets of the dorsum of *H. suspectum*, *P. apodus* and *C. zebrata*, Liang *et al.* (2021) found that the skin of the latter species absorbed the most energy. They suggested that it was related with the compound nature of the osteoderm. Our histology and 'tensile' test showed that temporal osteoderms of *C. zebrata* are relatively elastic, compared to those of *P. apodus* and *H. suspectum*, and have only a thin layer of capping tissue (Fig. 8). These observations are particularly interesting given that *C. zebrata* is the only arboreal species in our sample and is potentially at risk of falling. However, the stiffness of *C. zebrata* osteoderms *in toto* was intermediate between that of *H. suspectum* and *P. apodus*. Moreover, the osteoderms of *C. zebrata* did not stand out when it came to their response to dynamic loadings. Since the shape, size and imbrication pattern differ between the temporal, ventral and dorsal skin areas of every species studied, investigating the ventral and dorsal osteoderms *in toto* and using 'Tensile' tests may help improve our understanding of the interspecific differences in the biomechanical properties and energy absorption of the lizard skin.

When we consider biomechanical properties of lizard osteoderms it is important to keep in mind that they are only one part of a complex skin system. Our study showed that external loading of neighbouring osteoderms generally causes larger tensile than compressive strains in the instrumented osteoderm, with the exception of *H. suspectum* (Fig. 9). Overall however, our force transmission data did not reveal any obvious phylogenetic or morphological trends. For example, *H. horridum* showed a pattern of compressive and tensile strains distinct from the morphologically similar sister taxon *H. suspectum.* Since differences during development have been reported for helodermatid osteoderms (Moss, 1969) we cannot exclude the possibility that intraspecific rather than interspecific variations caused the observed differences. Further, given the large amount of overlap between osteoderms, we were expecting a proportionally greater transmission of force between the temporal osteoderms of *Tiliqua rugosa* and *P. apodus* compared to the other studied species (Fig. 1A). However, neither species demonstrated relatively high levels of force transmission during static loading, and only *Tiliqua rugosa* showed high force transmission levels during the dynamic loading. Force transmission during dynamic loading was also relatively high in the two *Heloderma* species, but relatively low in *P. apodus*, *C. zebrata*, and *Tribolonotus gracilis*¸ which had stiff and elastic osteoderms, respectively. We therefore hypothesize that force transmission during dynamic loading is only partly impacted by the stiffness of the osteoderms. Force transmission between osteoderms is probably impacted by several other factors, including the presence and organization of the large collagen bundles (Sharpey's fibers) that anchor the osteoderm within the skin (and interconnected osteodermites of compound osteoderms; see Williams et al., 2021). In order to better understand what role (if any) Sharpey's fibres and other microstructural components

play in the context of force transmission, future investigations integrating detailed histological descriptions and functional analyses are needed.

Other anatomical features of the head (*e.g.* muscle and bones of the skull) likely impacted our results as well. For example, the osteoderms located ventrally or posteriorly to the instrumented osteoderm were more often positioned adjacent to jaw muscles, while the anterior and dorsal osteoderms generally covered parts of the skull. We observed that larger strains were generally recorded from osteoderms that covered muscles (Fig. 3), suggesting that the nature of the underlying tissue could greatly impact the transmission of force between neighbouring osteoderms. Since we worked on fixed specimens, the underlying muscles were probably stiffer than they would have been in live animals, thus possibly leading to an overestimation of the stiffness of the skin system *in toto*. On the other hand, live individuals may be able to increase the stiffness of their skin by contracting the jaw adductor muscles. Additional experiments should be conducted on anesthetized and live specimens to investigate this topic further.

Evolutionary and ecological considerations

Based on our sample, it is impossible to formally assess the degree to which biomechanical properties of osteoderms are conserved among and between the different clades of lizards. It is, however, worth mentioning that we observed large differences in osteoderm stiffness between species of *Tiliqua* and *Tribolonotus* but not between the two helodermatids nor the two gerrhosaurids.

Stiffer osteoderms could be advantageous during conspecific fighting and/or interspecific interactions with predators or prey by preventing lethal or sublethal injuries. On the other hand, they most likely represent higher maintenance and energetic costs, and may impair locomotor performance (*e.g.* higher mass resulting in a lower endurance, lower flexibility possibly reducing mobility in fossorial species). The trade-off observed between locomotor performances and the degree of armature in cordylid lizards (Losos et al., 2002) provides some evidence for this.

In our sampling, osteoderms are confined to the head only in *Timon lepidus* but cover large or most parts of the body and head in the other species. *Timon lepidus* is likely the fastest lizard among the studied species (see Beck et al., 1995; Gans & Gasc, 1990; John-Alder et al., 1986; Main & Bull, 2000; Van Damme & Vanhooydonck, 2001; Vanhooydonck et al., 2014 for max. sprint speeds), suggesting that evolutionary constrains related with speed are probably stronger than those favouring skin stiffness of the body in this species. Such differences in osteoderm distribution as well

as those reported in this study for osteoderm stiffness could be related with interspecific differences in the balance between selective pressures associated with locomotor performances and protection against external loads.

Conspecific bites near or on the head have been reported for most of the studied species (e.g. Beck, 1990; Beck and Ramirez-Bautista, 1991; Jablonski, 2018; McCoy, 2006; Turner, 2010) or some of their close relatives (Pietruszka, 1988). In *Tiliqua rugosa*, conspecific bites to the head are common during male fights, often causing scale damages and sometimes breaking bones like the mandible (Kerr and Bull, 2002; Murray and Bull, 2004). Considering the stiff temporal osteoderms of that species, we hypothesized that stiff temporal osteoderms evolved in species capable of strong bites during interactions with conspecifics. A rapid evaluation of the bite forces recorded for eight out of the 11 species investigated here (Fig. S4) suggests that the data do not unequivocally support this hypothesis because there is no obvious correlation between temporal osteoderm stiffness and bite force; *H. suspectum* had low bite forces despite having stiff temporal osteoderms while *Tiliqua rugosa*, *Tiliqua scincoides* and *C. zebrata* had strong bites of similar magnitudes despite the differences in the stiffness of their osteoderms. In addition, both *Heloderma* species have stiff osteoderms although their fights are highly ritualized compared with that observed in most other lizards (Beck & Ramirez-Bautista, 1991). We would expect that ritualized fights reduce the occurrence of biting during agonistic interactions. Data suggest that this could be true for *H. suspectum* where bites are occasional, but not for *H. horridum* where the males can bite each other tenaciously and the dominant individual typically bites the jaw of the subordinate male at the end of each fighting bout, sometimes causing bleeding (Beck and Ramirez-Bautista, 1991). In this respect, it may be relevant that the lower jaw is covered with osteoderms in *H. horridum* but not in *H. suspectum* (Fig.1). Again, more morphological, behavioural and biomechanical data from a much larger sample of species would be needed to formally test our hypothesis but the data available suggest that the functional roles of osteoderms are likely diverse.

Conclusions and perspectives

Temporal osteoderms show interspecific differences in their stiffness and those differences can be quantified using strain gauges. Specimens investigated here were all formalin fixed which mostly likely increased the stiffness of the osteoderms and the underlying tissues. Therefore, differences in strains recorded for this study should be considered as relative differences. Future studies should explore strains in osteoderms of fresh specimens but also record strains during *in vivo* experiments to improve our understanding of the biomechanical properties and the ecological role of

osteoderms. Our discussion also highlights the need for more ecological data in order to be able to interpret the functional role(s) of the lizard osteoderms

Acknowledgments

We are very grateful to Prof. Callum Ross and Prof. Boris P. Chagnaud who provided templates and help during the writing of our Igor procedures. Prof. Ross and Ludovic Hallery (Vishay Group) also provided helpful tips for the recording of strain data. We also thank Dr. Nicolas Vidal and Dr. Marc Herbin who provided the specimens from the collections of the MNHN. We are also thankful to Kelia Isalas for her help with the 'Tensile test' experiment.

Competing interests

The authors declare that they have no competing interests.

Funding

This work was funded by a Human Frontier Science Program (RGP0039/2019).

References

Arnold, E. N. (1973). Relationships of the palaearctic lizards assigned to the genera Lacerta, Algyroides and Psammodromus (Reptilia: Lacertidae). *Bull. Br. Museum (Natural Hist. Zool.* **25**, 289–366.

Arnold, E. N. (1989). Towards a phylogeny and biogeography of the Lacertidae: relationships within an old-world family of lizards derived from morphology. *Bull. Br. Museum (Natural Hist. Zool.* **55**, 209–257.

Bates, D., Maechler, M., Bolker, B. and Walker, S. (2018). Fitting linear mixed-effects models using lme4. *J. Stat. Softw.* **67**, 1–48.

Beck, D. D. (1990). Ecology and behavior of the Gila monster in southwestern Utah. *J. Herpetol.* **24**, 54–68.

Beck, D. and Ramirez-Bautista, A. (1991). Combat behavior of the beaded lizard, *Heloderma h . horridum*, in Jalisco, México. *J. Herpetol.* **25**, 481–484.

Beck, D. D., Dohm, M. R., Garland, T., Ramírez-Bautista, A. and Lowe, C. H. (1995). Locomotor performance and activity energetics of helodermatid lizards. *Copeia* **3**, 577–585.

Broeckhoven, C. (2022). Intraspecific competition : a missing link in dermal armour evolution ? *J. Anim. Ecol.* 0–1.

Broeckhoven, C. and du Plessis, A. (2022). Osteoderms as calcium reservoirs : Insights from the lizard *Ouroborus cataphractus*. *J. Anat.* 1–6.

Broeckhoven, C., Diedericks, G. and Mouton, P. le F. N. (2015). What doesn't kill you might make you stronger: functional basis for variation in body armour. *J. Anim. Ecol.* **84**, 1213–1221.

Broeckhoven, C., du Plessis, A. and Hui, C. (2017). Functional trade-off between strength and thermal capacity of dermal armor: insights from girdled lizards. *J. Mech. Behav. Biomed. Mater.* **74**, 189–194.

Broeckhoven, C., El Adak, Y., Hui, C., Van Damme, R. and Stankowich, T. (2018a). On dangerous ground: the evolution of body armour in cordyline lizards. *Proc. R. Soc. B Biol. Sci.* **285**,.

Broeckhoven, C., Mouton, P. le F. N. and Hui, C. (2018b). Proximate causes of variation in dermal armour: insights from armadillo lizards. *Oikos* **127**, 1449–1458.

Canei, J. and Nonclercq, D. (2020). Morphological study of the integument and corporal skeletal muscles of two psammophilous members of Scincidae (*Scincus scincus* and *Eumeces schneideri*). *J. Morphol.* **282**, 230–246.

Carrier, D. R. and Morgan, M. H. (2014). Protective buttressing of the hominin face. *Biol. Rev.* **90**, 330–346.

Clarac, F., Goussard, F., De Buffrénil, V. and Sansalone, V. (2019). The function(s) of bone ornamentation in the crocodylomorph osteoderms: A biomechanical model based on a finite element analysis. *Paleobiology* **45**, 182–200.

Connors, M., Yang, T., Hosny, A., Deng, Z., Yazdandoost, F., Massaadi, H., Eernisse, D., Mirzaeifar, R., Dean, M. N., Weaver, J. C., et al. (2019). Bioinspired design of flexible armor based on chiton scales. *Nat. Commun.* **10**, 1–13.

Dutel, H., Gröning, F., Sharp, A. C., Watson, P. J., Herrel, A., Ross, C. F., Jones, M. E. H., Evans, S. E. and Fagan, M. J. (2021). Comparative cranial biomechanics in two lizard species: impact of variation in cranial design. *J. Exp. Biol.* **224**, jeb234831.

Gans, C. and Gasc, J. (1990). Tests on the locomotion of the elongate and limbless reptile *Ophisaurus apodus* (Sauria : Anguidae). *J. Zool.* **220**, 517–536.

Grassi, L. and Isaksson, H. (2015). Extracting accurate strain measurements in bone mechanics: a critical review of current methods. *J. Mech. Behav. Biomed. Mater.* **50**, 43–54.

Herrel, A., Spithoven, L., Van Damme, R. and De Vree, F. (1999). Sexual dimorphism of head size in *Gallotia galloti*: testing the niche divergence hypothesis by functional analyses. *Funct. Ecol.* **13**, 289–297.

Hylander, W. L. (1984). Stress and strain in the mandibular symphysis of primates: a test of competing hypotheses. *Am. J. Phys. Anthropol.* **64**, 1–46.

Hylander, W. L. and Johnson, K. R. (1997). *In vivo* bone strain patterns in the zygomatic arch of macaques and the significance of these patterns for functional interpretations of craniofacial form. *Am. J. Phys. Anthropol.* **102**, 203–232.

Hylander, W. L., Johnson, K. R. and Picq, P. G. (1991). Masticatory-stress hypotheses and the supraorbital region of primates. *Am. J. Phys. Anthropol.* **86**, 1–36.

Iacoviello, F., Kirby, A. C., Javanmardi, Y., Moeendarbary, E., Shabanli, M., Tsolaki, E., Sharp, A. C., Hayes, M. J., Keevend, K., Li, J. H., et al. (2020). The multiscale hierarchical structure of *Heloderma suspectum* osteoderms and their mechanical properties. *Acta Biomater.* **107**, 194–203.

Inacio Veenstra, L. L. and Broeckhoven, C. (2022). Revisiting the thermoregulation hypothesis of osteoderms : a study of the crocodilian *Paleosuchus palpebrosus* (Crocodilia : Alligatoridae). *Biol. J. Linn. Soc.* **135**, 679–691.

Jablonski, D. (2018). Male-male combat in *Pseudopus apodus* (Repitilia: Anguidae). *Russ. J. Herpetol.* **25**, 293–298.

Jennings, A. R. (2009). An analysis of 1,000 deaths in wild birds. *Bird Study* **8**, 26–31.

John-Alder, H. B., Garland, T. J. and Bennett, A. F. (1986). Locomotory capacities, oxygen consumption, and the cost of locomotion of the shingle-back lizard (Trachydosaurus rugosus). *Physiol. Zool.* **59**, 523–531.

Kerr, G. D. and Bull, C. M. (2002). Field observations of aggressive encounters between male sleepy lizards (*Tiliqua rugosa*). *Herpetol. Rev.* **33**, 24–26.

Kirby, A., Vickaryous, M., Boyde, A., Olivo, A., Moazen, M., Bertazzo, S. and Evans, S. (2020). A comparative histological study of the osteoderms in the lizards *Heloderma suspectum* (Squamata: Helodermatidae) and *Varanus komodoensis* (Squamata: Varanidae). *J. Anat.* 1–9.

Laver, R. J., Morales, C. H., Heinicke, M. P., Gamble, T., Longoria, K., Bauer, A. M. and Daza, J. D. (2020). The development of cephalic armor in the tokay gecko (Squamata: Gekkonidae: *Gekko gecko*). *J. Morphol.* **281**, 213–228.

Liang, C., Marghoub, A., Kever, L., Bertazzo, S., Abzhanov, A., Vickaryous, M., Herrel, A., Evans, S. and Moazen, M. (2021). Lizard osteoderms – morphological characterisation, biomimetic design and manufacturing based on three species. *Bioinspir. Biomim.* **16**, 1–11.

Losos, J. B., Mouton, P. L. F. N., Bickel, R., Cornelius, I. and Ruddock, L. (2002). The effect of body armature on escape behaviour in cordylid lizards. *Anim. Behav.* **64**, 313–321.

Main, A. R. and Bull, M. (2000). The impact of tick parasites on the behaviour of the lizard *Tiliqua rugosa*. *Oecologia* **122**, 574–581.

Marghoub, A., Williams, C. J. A., Leite, J. V., Kirby, A. C., Kéver, L., Porro, L. B., Barett, P. M., Bertazzo, S., Abzhanov, A., Vickaryous, M., et al. (2022). Unravelling the structural variation of lizard osteoderms. *Acta Biomater.* **in press**,.

Markey, M. J., Main, R. P. and Marshall, C. R. (2006). In vivo cranial suture function and suture morphology in the extant fish *Polypterus*: implications for inferring skull function in living and fossil fish. *J. Exp. Biol.* **209**, 2085–2102.

Marques, M. P., Ceríaco, L. M. P., Stanley, E. L., Bandeira, S. A., Agarwal, I. and Bauer, A. M. (2019). A new species of girdled lizard (Squamata: Cordylidae) from the Serra da Neve Inselberg, Namibe Province, southwestern Angola. *Zootaxa* **4668**, 503–524.

McCoy, M. (2006). *Reptiles of the Solomon Islands*. Sofia, Bulgaria: Pensoft Publisher.

Metzger, K. A., Daniel, W. J. T. and Ross, C. F. (2005). Comparison of beam theory and finite-element analysis with in vivo bone strain data from the alligator cranium. *Anat. Rec. PART A* **283A**, 331–348.

Moss, M. . (1969). Comparative histology of dermal sclerifications. *Acta Anat. (Basel).* **73**, 510–533.

Mukherjee, S. and Heithaus, M. R. (2013). Dangerous prey and daring predators: a review. *Biol. Rev.* **88**, 550–563.

Murray, K. and Bull, C. M. (2004). Aggressiveness during monogamous pairing in the sleepy lizard, *Tiliqua rugosa* : a test of the mate guarding hypothesis. *Acta Ethol.* **7**, 19–27.

Oliver, J. A. (1951). Ontogenetic changes in osteodermal ornamentation in skinks. *Copeia* **1951**, 127.

Paluh, D. J., Griffing, A. H. and Bauer, A. M. (2017). Sheddable armour: identification of osteoderms in the integument of *Geckolepis maculata* (Gekkota). *African J. Herpetol.* **66**, 12–24.

Pietruszka, R. D. (1988). Observations on sexual dimorphism and social structure in the lizard *Angolosaurus skoogi* (Cordylidae) of the northern Namib Desert dunes. *South African J. Zool.* **23**, 47–51.

Porro, L. B., Metzger, K. A., Iriarte-Diaz, J. and Ross, C. F. (2013). *In vivo* bone strain and finite element modeling of the mandible of *Alligator mississippiensis*. *J. Anat.* **223**, 195–227.

Porro, L. B., Ross, C. F., Iriarte-Diaz, J., O'Reilly, J. C., Evans, S. E. and Fagan, M. J. (2014). *In vivo* cranial bone strain and bite force in the agamid lizard Uromastyx geyri. *J. Exp. Biol.* **217**, 1983–1992.

Ross, C. F., Porro, L. B., Herrel, A., Evans, S. E. and Fagan, M. J. (2018). Bite force and cranial bone strain in four species of lizards. *J. Exp. Biol.* **221**,.

Smith, K. K. and Hylander, W. L. (1985). Strain gauge measurement of mesokinetic movement in the lizard *Varanus exanthematicus*. *J. Exp. Biol.* **114**, 53–70.

Song, J., Ortiz, C. and Boyce, M. C. (2011). Threat-protection mechanics of an armored fish. *J. Mech. Behav. Biomed. Mater.* **4**, 699–712.

Stanley, E. L. (2013). Systematics and morphological diversification of the Cordylidae (Squamata).

Strahm, M. H. and Schwartz, A. (1977). Osteoderms in the anguid lizard subfamily Diploglossinae and their taxonomic importance. *Biotropica* **9**, 58–72.

Tanke, D. H. and Currie, P. J. (1998). Head-biting behavior in thetrapod dinosaurs: paleopathological evidence. *Gaia* **184**, 167–184.

Team, R. D. C. (2016). R: A language and environment for statistical computing.

Thomas, N. J. and Cole, R. A. (1996). The risk of disease and threats to the wild population. *Endanger. Species Updat.* **13**, 23–27.

Thomason, J. J. (1991). Cranial strength in relation to estimated biting forces in some mammals. *Can. J. Zool.* **69**, 2326–2333.

Tonini, J. F. R., Beard, K. H., Ferreira, R. B., Jetz, W. and Pyron, R. A. (2016). Fully-sampled phylogenies of squamates reveal evolutionary patterns in threat status. *Biol. Conserv.* **204**, 23–31.

Turner, G. S. (2010). Natural history notes on the eastern blue-tongued skink *Tiliqua scincoides* scincoides from the basalt plains around Melbourne. *Vic. Nat.* **127**, 71–78.

Van Damme, R. and Vanhooydonck, B. (2001). Origins of interspecific variation in lizard sprint capacity. *Funct. Ecol.* **15**, 186–202.

Vanhooydonck, B., James, R. S., Tallis, J., Aerts, P., Tadic, Z., Tolley, K. A., Measey, G. J. and Herrel, A. (2014). Is the whole more than the sum of its parts ? Evolutionary trade-offs between burst and sustained locomotion in lacertid lizards. *Proc. R. Soc. B* **281**, 2132677.

Vickaryous, M. K. and Sire, J. Y. (2009). The integumentary skeleton of tetrapods: origin, evolution, and development. *J. Anat.* **214**, 441–464.

Weijs, W. A. and De Jongh, H. J. (1977). Strain in mandibular alveolar bone during mastication in the rabbit. *Arch. Oral Biol.* **22**, 667–675.

Williams, C., Kirby, A., Marghoub, A., Kéver, L., Ostashevskaya-gohstand, S., Bertazzo, S., Moazen, M., Abzhanov, A., Herrel, A., Evans, S. E., et al. (2021). A review of the osteoderms of lizards (Reptilia : Squamata). *Biol. Rev.* **97**, 1–19.

Yang, W., Chen, I. H., Gludovatz, B., Zimmermann, E. A., Ritchie, R. O. and Meyers, M. A. (2013). Natural flexible dermal armor. *Adv. Mater.* **25**, 31–48.

Zylberberg, L. and Castanet, J. (1985). New data on the structure and the growth of the osteoderms in the reptile *Anguis fragilis* L. (Anguidae, Squamata). *J. Morphol.* **186**, 327–342.

Figures and Table

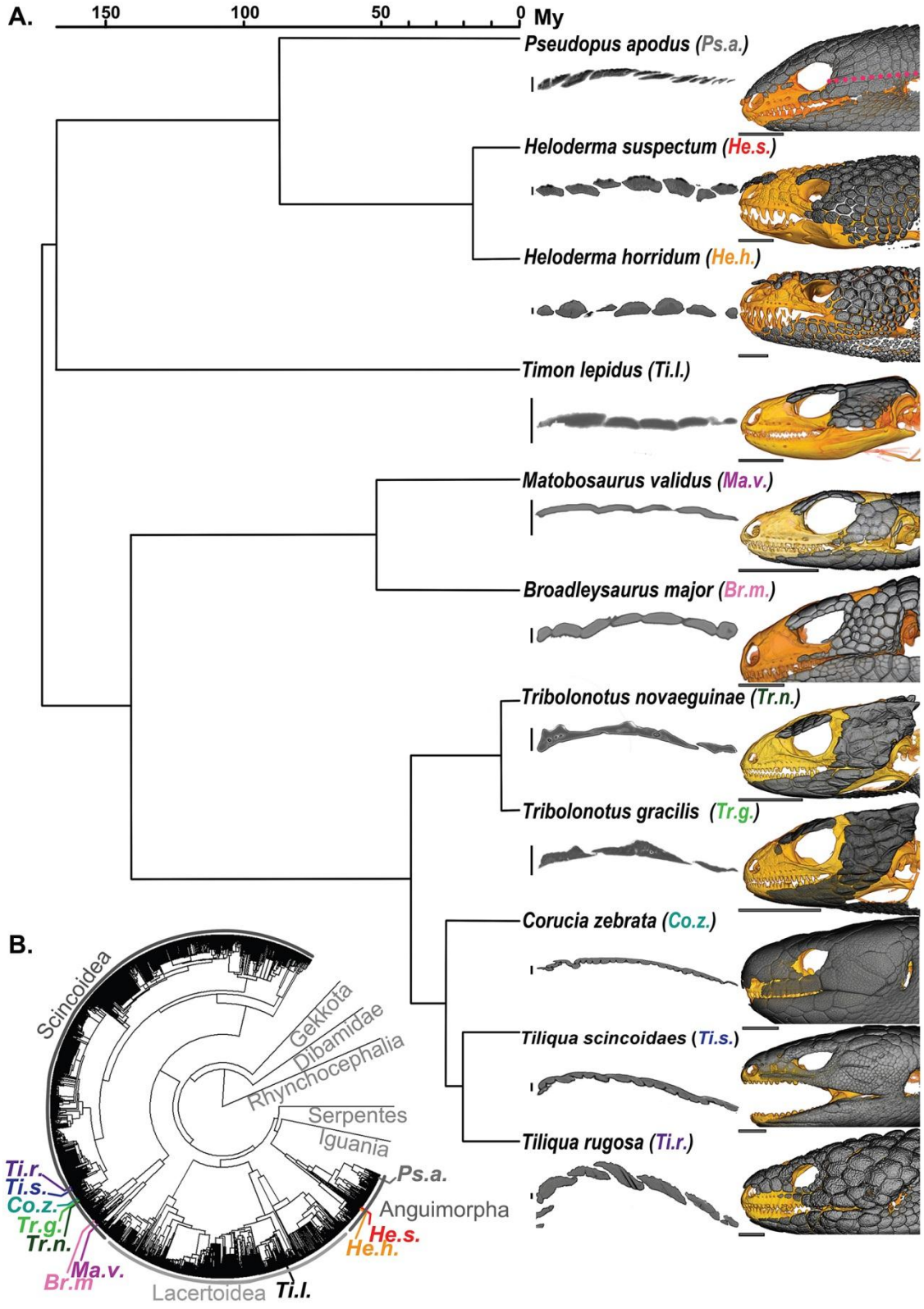

Fig. 1. Distribution, phylogenetic relationships, and osteoderm morphology of the studied species. A. Phylogenetic relationships (left, based on Tonini et al., 2016) and morphology of the temporal osteoderms in the sampled species. 3D reconstruction of the skull (orange-yellow) and head osteoderms (gray) of the eleven species (right). Virtual longitudinal section (middle) through temporal osteoderms from a ventral view and along the rostro-caudal axis (illustrated by the dotted magenta line on the 3D reconstruction of the *P. apodus* head). B. Distribution of the sampled species within Lepidosauria. Scale bars: 1 mm (vertical black bar) and 1 cm (horizontal black and grey bar). Except for *Pseudopus apodus* (MNHN, FUNEVOL virtual collection) and *Heloderma suspectum* (UCL, Evans Lab), µCT raw images from the studied species were downloaded from MorphoSource (*Heloderma horridum*: ark:/87602/m4/M98538, oUTCT, funded by NSF EF-0334961. *Timon lepidus*: ark:/87602/m4/M72278, Yale Peabody Museum, funded by NSF DBI-1701714; NSF DBI-1702263; overt TCN; NSF DBI-1701769. *Broadleysaurus major*: ark:/87602/m4/M74672, California Academy of Sciences, funded by oVert TCN. *Matobosaurus validus:* ark:/87602/m4/M71913, California Academy of Sciences, funded by oVert TCN. *Tribolonotus novaeguineae*: ark:/87602/m4/M61910, University of Michigan Museum of Zoology, funded by NSF DBI-1701714; NSF DBI-1701735; oVert TCN. *Tribolonotus* cf. *gracilis* (listed as *Tribolonotus* sp. on MorphoSource): ark:/87602/m4/M40298, The oVert Thematic Collections Network, funded by oVert Thematic Collections Network (TCN), NSF DBI-1701714. *Corucia zebrata*: ark:/87602/m4/M43624, California Academy of Sciences Herpetology collection, funded by oVert Thematic Collections Network (TCN), NSF DBI-1701714, 1701870. *Tiliqua scincoides*: ark:/87602/m4/M74717, funded by NSF DBI-1701714; NSF DBI-1701870; NSF DBI-1701713; oVert TCN. *Tiliqua rugosa*: ark:/87602/m4/M48823, Florida Museum of Natural History (University of Florida), funded by oVert TCN: NSF DBI1701714.

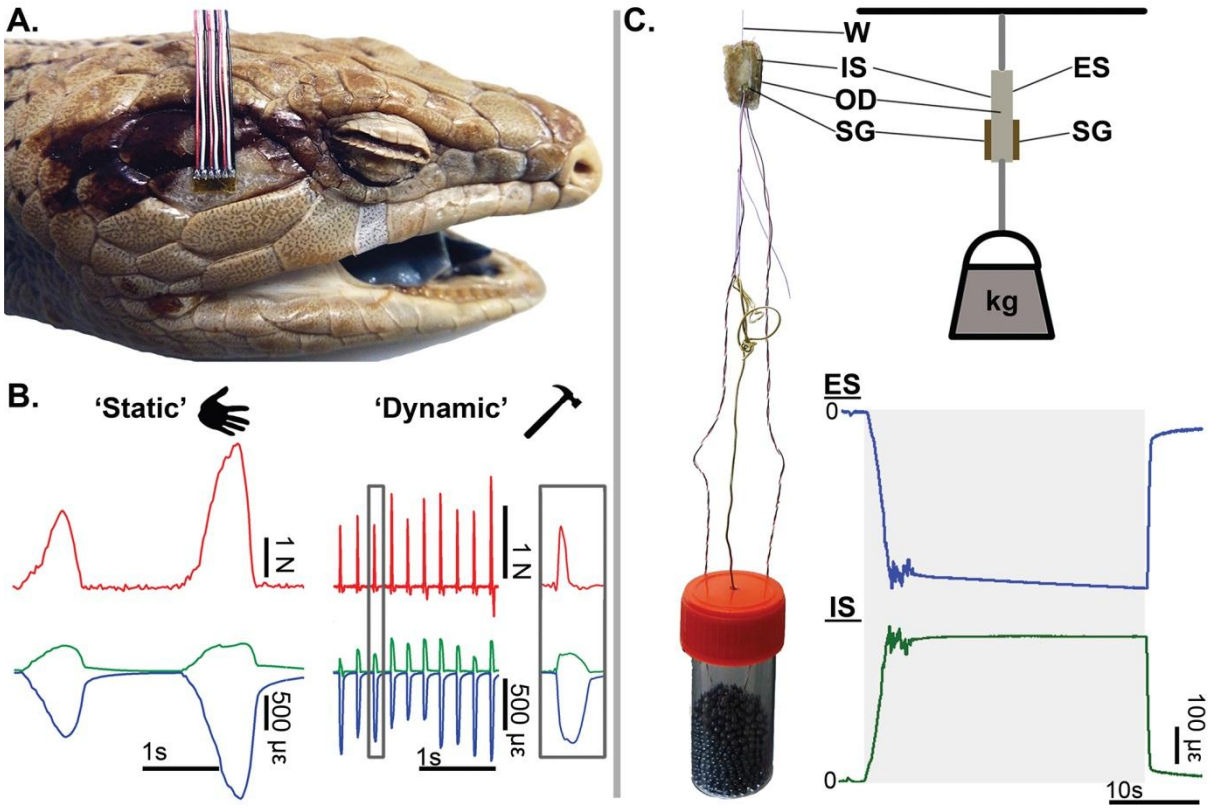

Fig. 2. Osteoderm loadings and strain recordings. A. Temporal osteoderm of a *Tiliqua scincoides* instrumented with a rectangular rosette strain gauge. Loadings were obtained either by manually pressing a pin mounted on a piezoelectric sensor or by using a small piezoelectric hammer. B. Illustration of the force (red), tensile (green) and compressive strain (blue) waveforms recorded during the experiment illustrated in A. The hand symbol illustrates the relatively 'static' loading obtained when the pin was pressed manually while the hammer symbol means that the loading was more dynamic and obtained by using the piezoelectric hammer. C. 'Tensile' test experiment on a dissected osteoderm of *C. zebrata.* Picture (left) and schematic representation (top right) of the experimental setup. Waveforms recorded from the external and internal sides of the osteoderms using single element gauges. The grey area highlights the time period during which the osteoderm was loaded using a 200g weight. ES: external side of the dissected osteoderm. IS: internal side of the dissected osteoderm. OD: osteoderm. SG: single element gauge. W: wire used to hang the osteoderm.

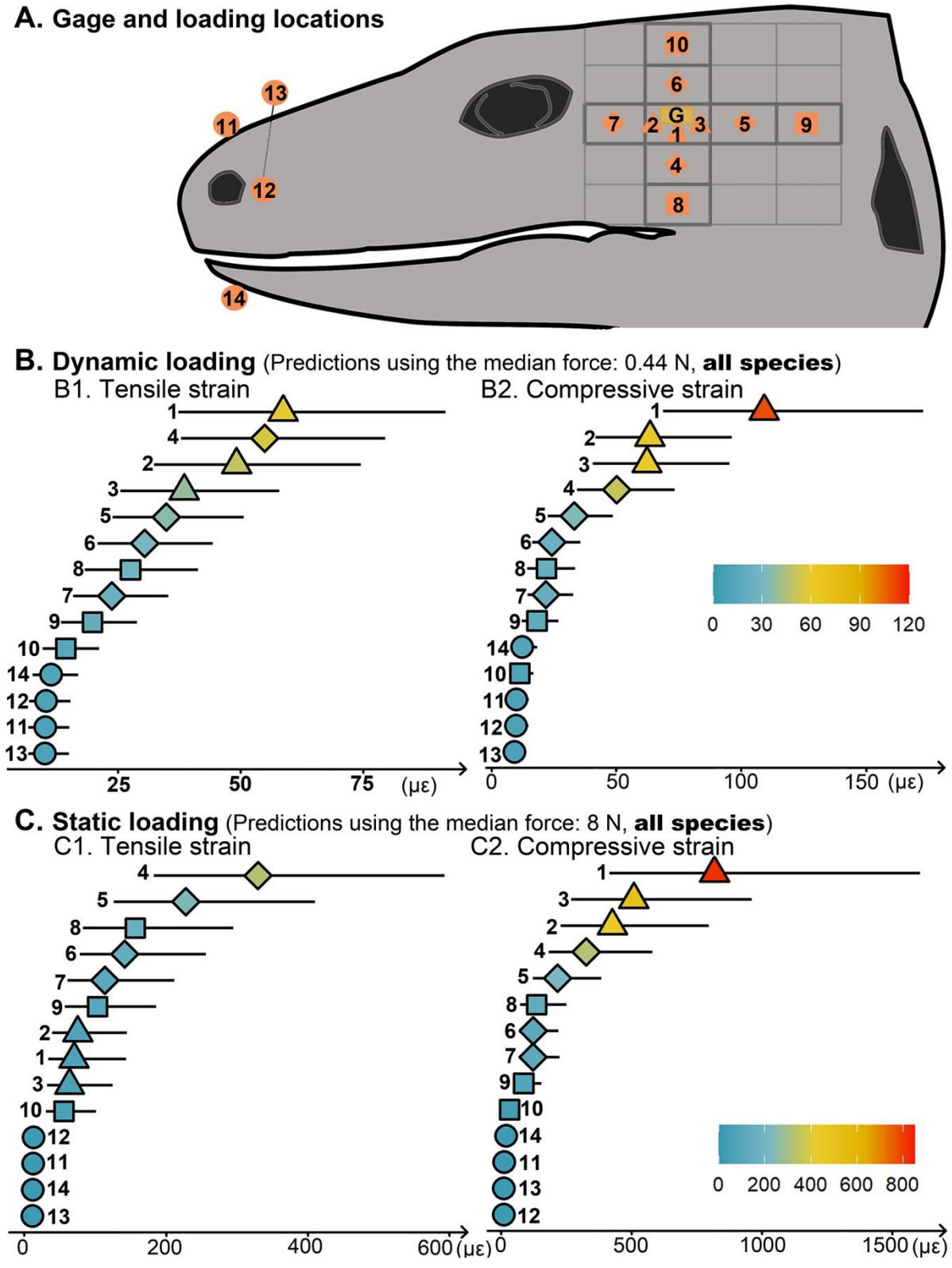

Fig. 3. Effect of the location of the loading on the strains predicted for the instrumented osteoderm. A. Location of the 14 different places where loading was applied. Locations are indicated by a triangle when force is applied directly on the instrumented osteoderm, a diamond when the

force is applied on an osteoderm adjacent to the instrumented osteoderm, a square when it is applied to an osteoderm separated from the instrumented osteoderm by one osteoderm, and a circle when it is applied near the rostral end of the head. B. Tensile and compressive strains predicted for each location by the Linear Mixed Model using the 'dynamic' data. C. Tensile and compressive strains predicted for each location by the Linear Mixed Model using the 'static' data.

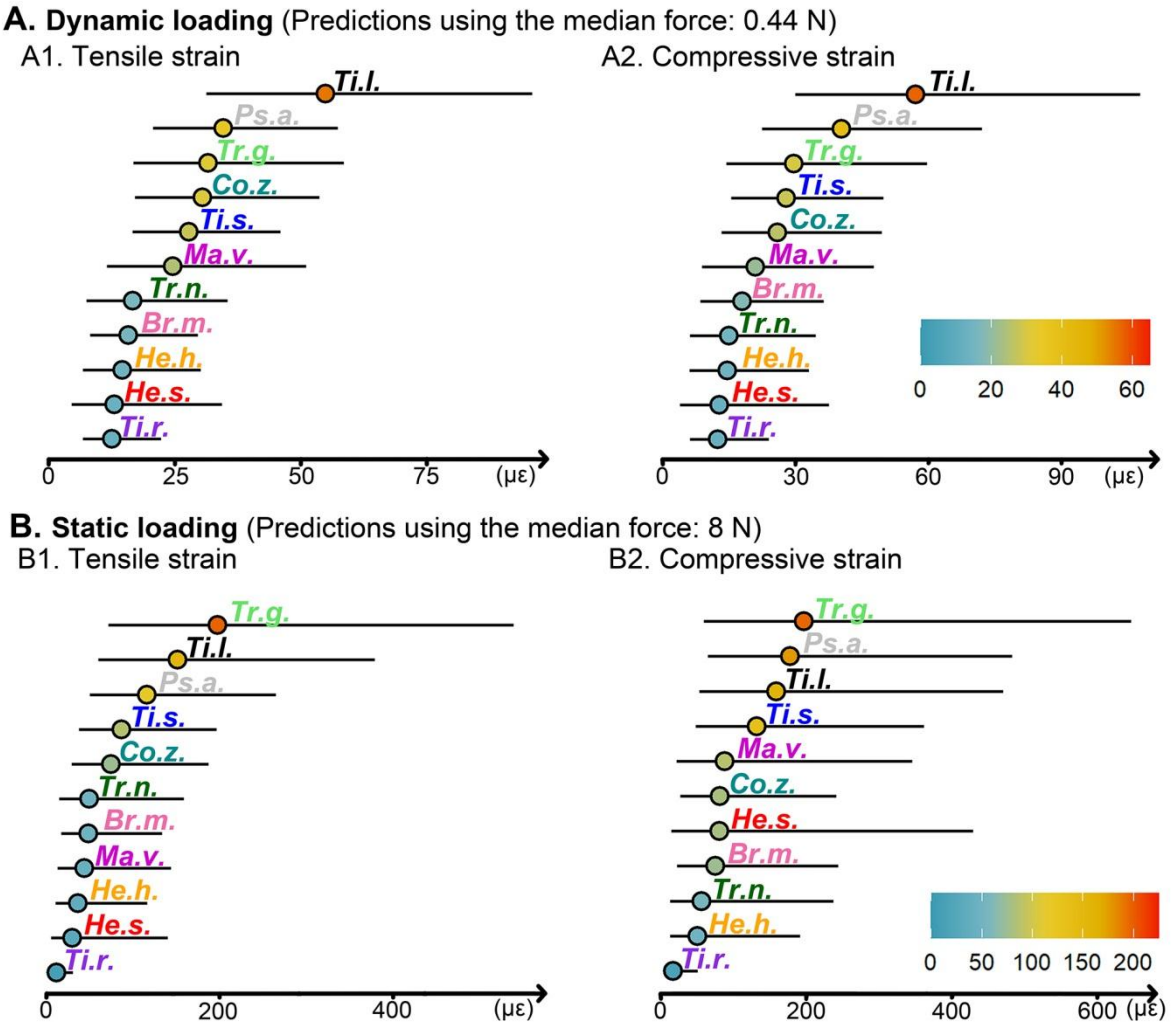

Fig. 4. *In-toto* interspecific differences in the stiffness of the skin system. The graphs show the strains predicted by the Linear Mixed Model for the instrumented osteoderm. The locations were included in the model as a random covariate. *Br.m: Broadleysaurus major. Co.z.: Corucia zebrata. He.h.: Heloderma horridum. He.s.: Heloderma suspectum. Ma.v.: Matobosaurus validus. Ps.a.: Pseudopus apodus. Ti.r.: Tiliqua rugosa. Ti.s.: Tiliqua scincoides. Ti.l.: Timon lepidus. Tr.g.: Tribolonotus gracilis. Tr.n.: Tribolonotus novaeguineae.*

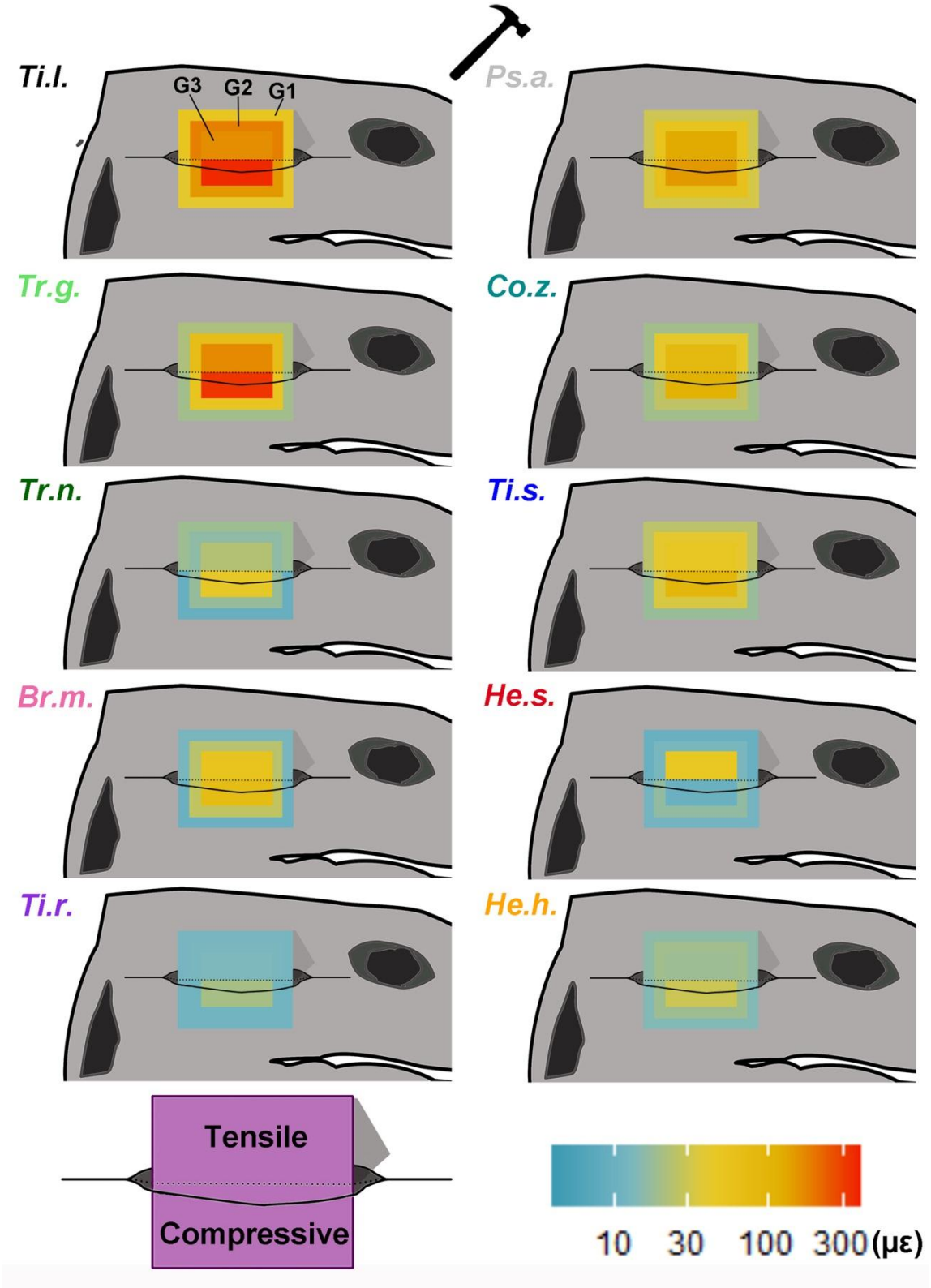

Fig. 5. Interspecific differences in stiffness depending on the location of the dynamic loading. G1: Loading on osteoderms (ODs) that are separated from the instrumented OD by one OD. G2: Loading on osteoderms (ODs) that are adjacent to the instrumented OD. G3: loading directly applied on the

instrumented OD. The upper half of each rectangle illustrates the predicted tensile strain while the lower half illustrates the predicted compressive strain. Strain magnitude is expressed using a color gradient. *Br.m: Broadleysaurus major. Co.z.: Corucia zebrata. He.h.: Heloderma horridum. He.s.: Heloderma suspectum. Ps.a.: Pseudopus apodus. Ti.r.: Tiliqua rugosa. Ti.s.: Tiliqua scincoides. Ti.l.*: *Timon lepidus. Tr.g.: Tribolonotus gracilis. Tr.n.: Tribolonotus novaeguineae.*

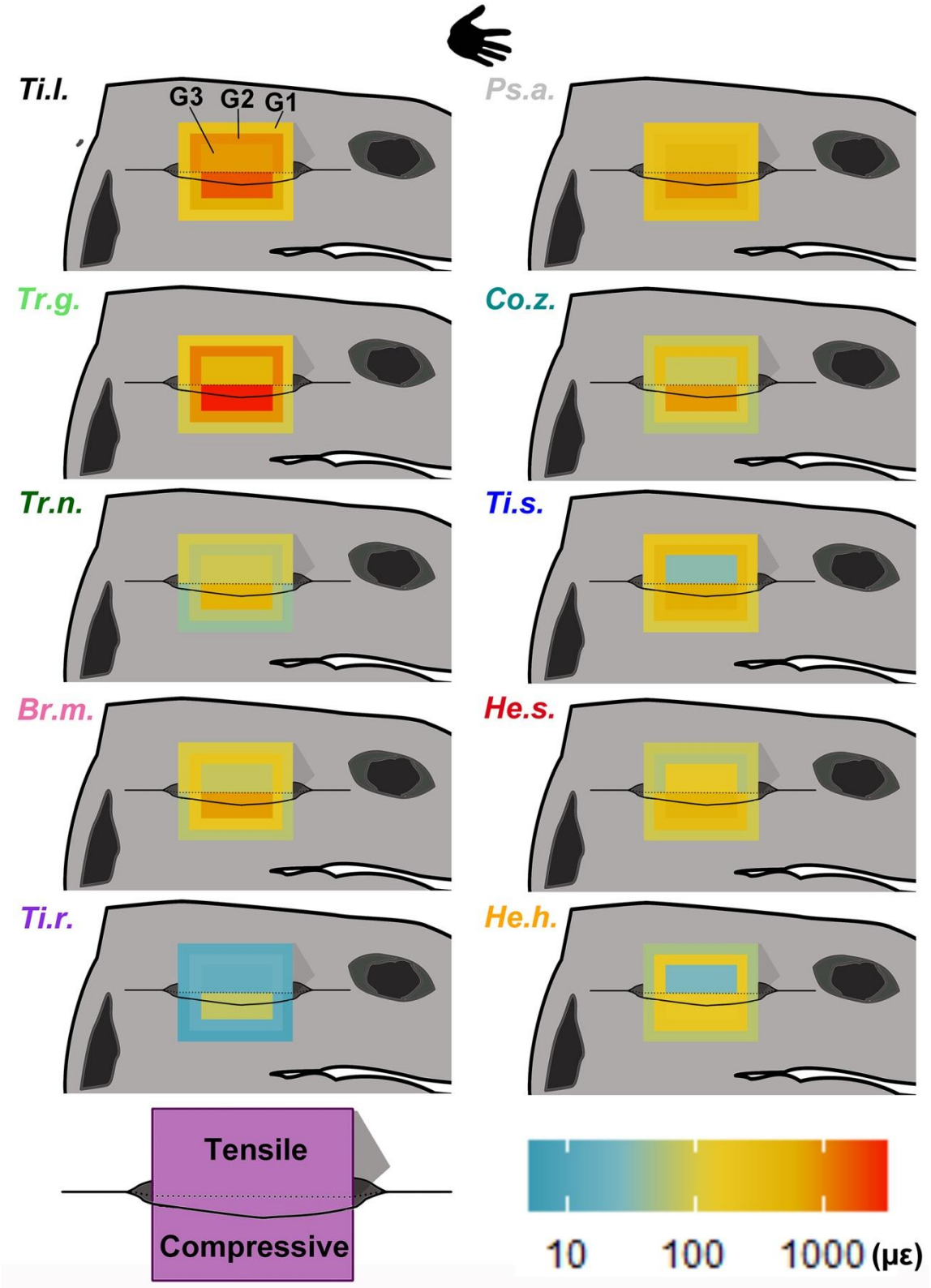

Fig. 6. Interspecific differences in the stiffness considering the location of the static loading. G1: Loading on osteoderms (ODs) that are separated from the instrumented OD by one OD. G2: Loading on osteoderms (ODs) that are adjacent to the instrumented OD. G3: loading directly applied on the

instrumented OD. The upper half of each rectangle illustrates the predicted tensile strain while the lower half illustrates the predicted compressive strain. Strain magnitude is expressed using a color gradient. *Br.m: Broadleysaurus major. Co.z.: Corucia zebrata. He.h.: Heloderma horridum. He.s.: Heloderma suspectum. Ps.a.: Pseudopus apodus. Ti.r.: Tiliqua rugosa. Ti.s.: Tiliqua scincoides. Ti.l.*: *Timon lepidus. Tr.g.: Tribolonotus gracilis. Tr.n.: Tribolonotus novaeguineae.*

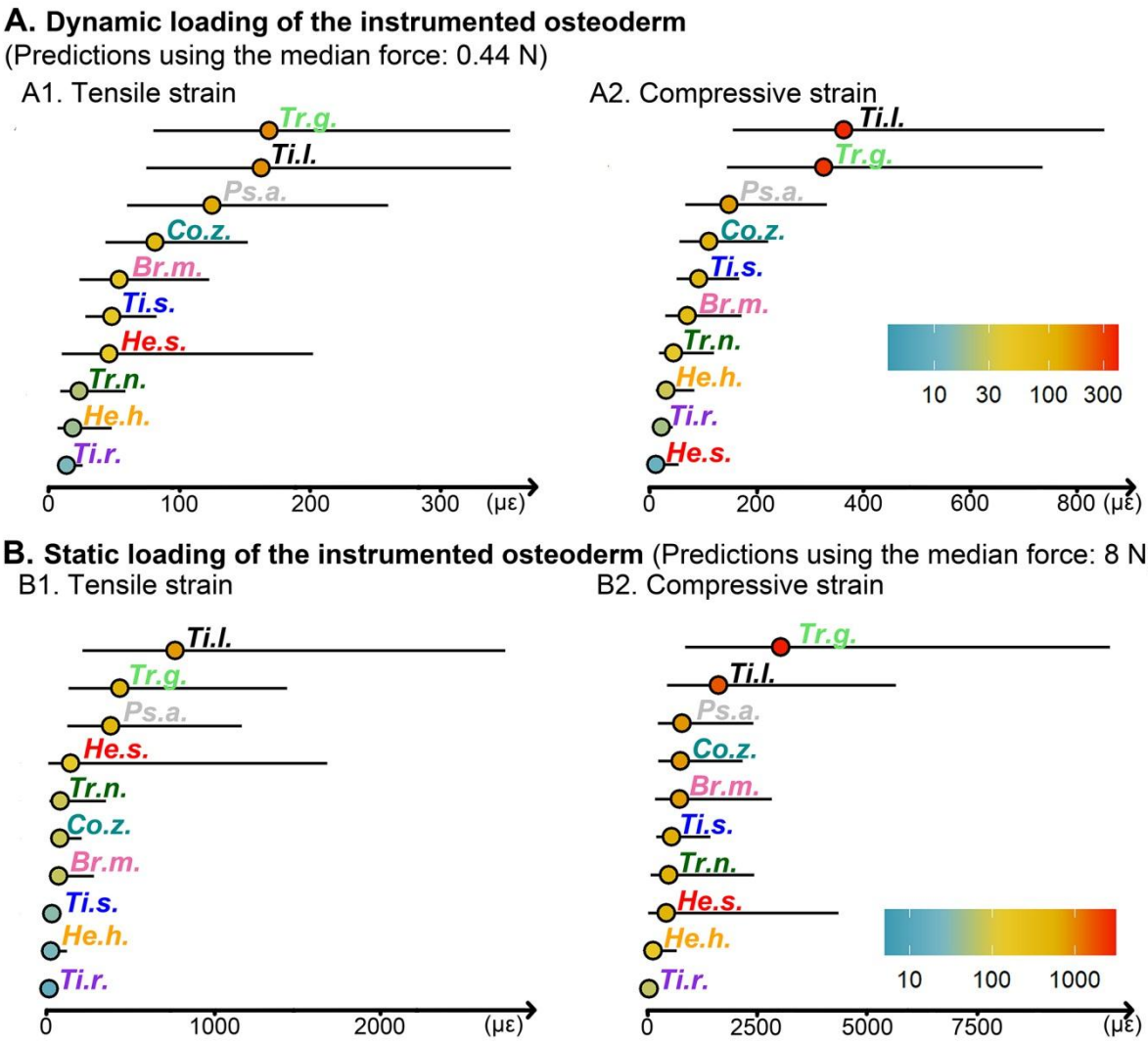

Fig. 7. *In toto* interspecific differences in the stiffness of the instrumented osteoderms. Strains predicted by the Linear Mixed Model considering only loading applied directly to the instrumented osteoderm *in toto*. *Br.m: Broadleysaurus major. Co.z.: Corucia zebrata. He.h.: Heloderma horridum. He.s.: Heloderma suspectum. Ma.v.: Matobosaurus validus. Ps.a.: Pseudopus apodus. Ti.r.: Tiliqua rugosa. Ti.s.: Tiliqua scincoides. Ti.l.*: *Timon lepidus. Tr.g.: Tribolonotus gracilis. Tr.n.: Tribolonotus novaeguineae.*

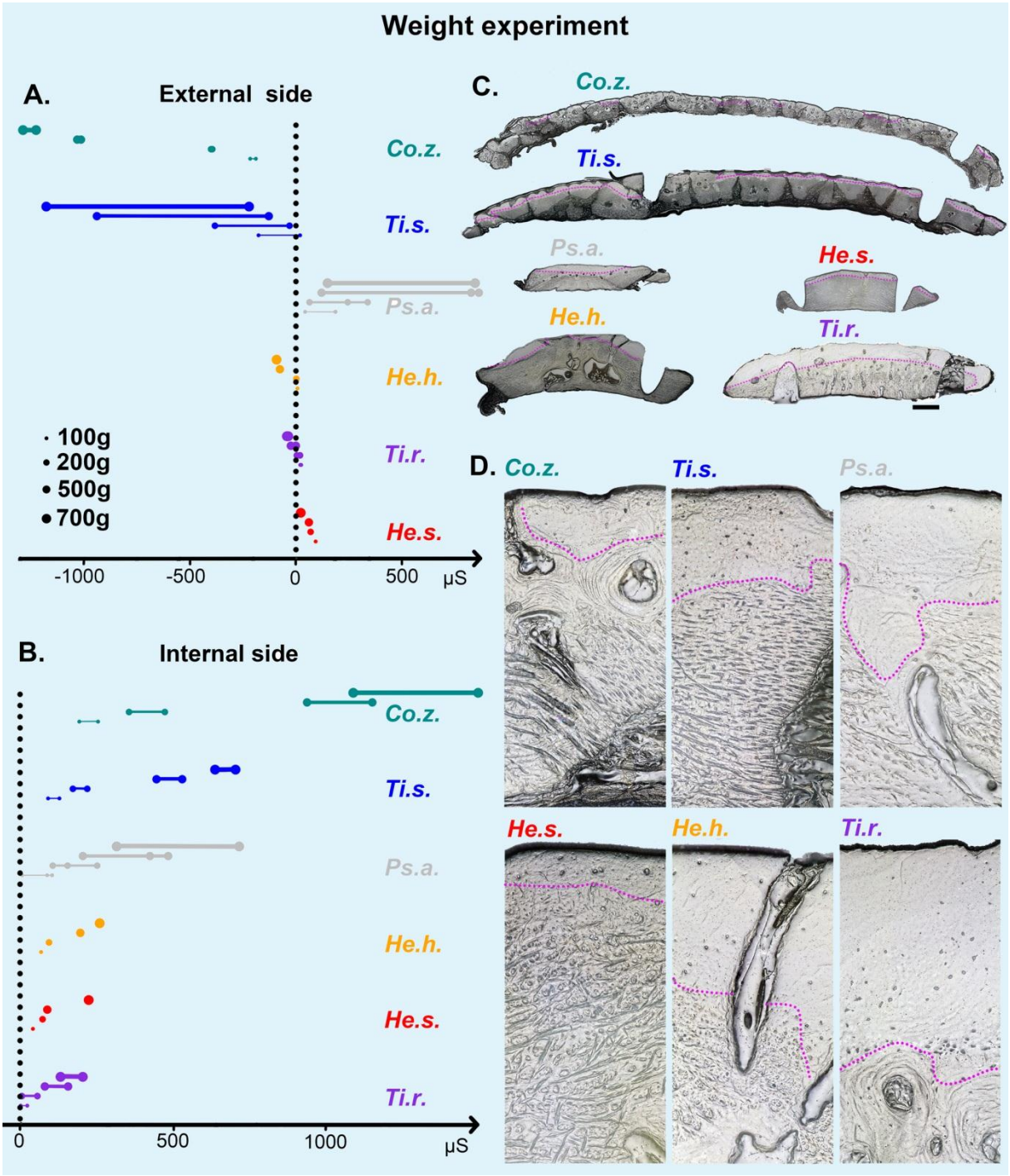

Fig. 8. Interspecific differences in the stiffness of dissected osteoderms. Tensile and compressive strains recorded from a subsample of dissected ODs. Here, the OD was loaded along its long axis using different weights (100, 200, 500, and 700g) and strains were recorded along that axis using single strain gauges placed on the external and internal sides of the OD. A. Strains recorded on the external side of the osteoderm. B. Strains recorded on the internal side of the osteoderm. C. Histological cross section of one dissected osteoderm per species. D. 500µm width insets of ODs

shown in C. Pink dotted lines highlight the limit of the capping tissue. Note that layer of capping tissue is generally thicker in *Heloderma suspectum* but the section presented here comes from the area that was trimmed to attach the strain gauge. *Co.z.: Corucia zebrata. He.h.: Heloderma horridum. He.s.: Heloderma suspectum. Ps.a.: Pseudopus apodus. Ti.r.: Tiliqua rugosa. Ti.s.: Tiliqua scincoides.* Scale: 1 mm.

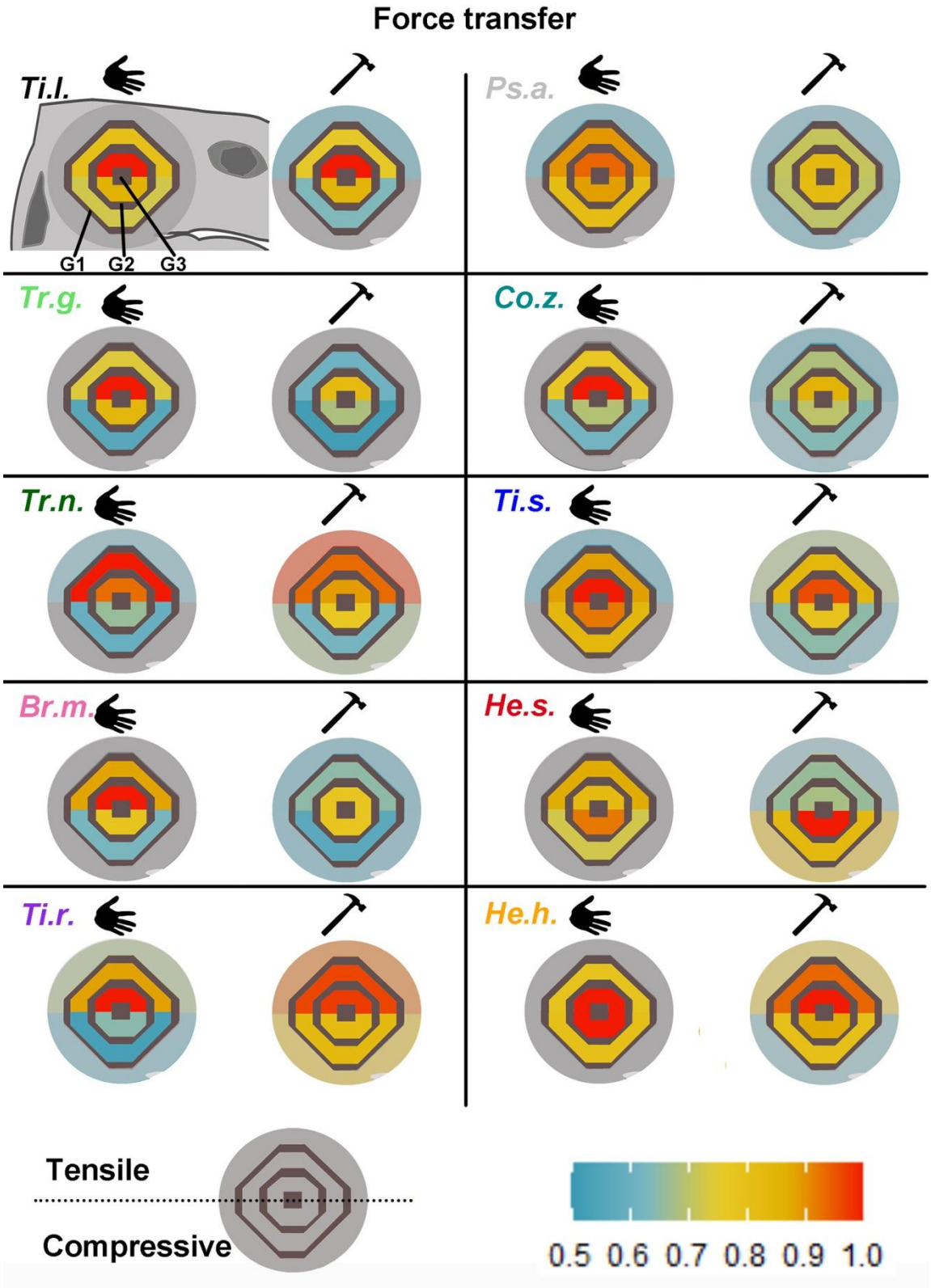

Fig. 9. Interspecific differences in the force transfer between adjacent osteoderms. Relative changes between the groups 1, 2 and 3 were calculated within each species and colour coded to determine whether there were interspecific differences in the relative amount of stress transmitted to the neighbouring osteoderms.

Table 1. Family, collection ID, gender, head length (HL), and Snout-Vent-Length (SVL) of the sampled specimens

Family	Species	Specimen	Collection ID	SVL (mm)	HL (mm)	Gender
Anguidae	*Pseudopus apodus* (PALLAS, 1775)	Psa_1	Herrel psa1	375	39	U
		Psa_2	MNHN 2619	418	45	M
		Psa_3	Herrel psa2 (head)	NA	36	U
		Psa_4	MNHN 1939 245	387	37	U
		Psa_5	MNHN 1912 355	342	35	U
		Psa_6	MNHN 1884 519	371	32	U
Helodermatidae	*Heloderma horridum* (WIEGMANN, 1829)	Heh_1	Herrel heh2	317	53	F
		Heh_2	MNHN 1201	271	47	F
	Heloderma suspectum (COPE, 1869)	Hes_1	MNHN 133138	259	44	U
		Hes_2	MNHN 1950 174	279	49	U
Lacertidae	*Timon lepidus* (DAUDIN, 1802)	Til_1	MNHN 1978 963	161	44	M
		Til_2	MNHN 1918-91	196	52	M
		Til_3	Herrel til1	149	41	M
		Til_4	MNHN 1922 325	119	33	M
Gerrhosauridae	*Broadleysaurus major* (DUMÉRIL, 1851)	Brm_1	MNHN 1050	194	38	M
		Brm_2	MNHN 2788	199	35	M
		Brm_3	MNHN 2786	211	34	M
	Matobosaurus validus (SMITH, 1849)	Mav_1	Herrel mav1	216	40	M
		Mav_2	MNHN: 1987 1813	209	48	M
Scincidae	*Corucia zebrata* (GRAY, 1855)	Coz_1	Herrel coz1	275	46	F
		Coz_2	Herrel coz2	211	45	F
		Coz_3	MNHN 1990-4733	270	58	F
		Coz_4	MNHN 4413	246	41	F
	Tiliqua rugosa (GRAY, 1825)	Tir_1	Herrel tir1	288	55	M
		Tir_2	Herrel tir2	275	44	F
		Tir_3	MNHN 9047	227	52	F
		Tir_4	MNHN 56-103	265	46	M
	Tiliqua scincoides (WHITE, 1790)	Tis_1	Herrel tis1	310	49	M
		Tis_2	Herrel tis2	230	47	M
		Tis_3	MNHN 94534	307	58	F
		Tis_4	MNHN 1982-511	284	54	F
		Tis_5	MNHN 1911-194	269	47	F

		Tis_6	MNHN 1904-140	250	45	F
	Tribolonotus gracilis (DE ROOIJ, 1909)	Trg_1	Herrel trg1	106	26	U
		Trg_2	Herrel trg2	109	24	U
		Trg_3	Herrel trg3	106	22	U
	Tribolonotus novaeguineae (SCHLEGEL, 1834)	Trn_1	Herrel trn1	103	22	U
		Trn_2	Herrel trn2	90	22	U

F: Female. M: Male. U: Undetermined.

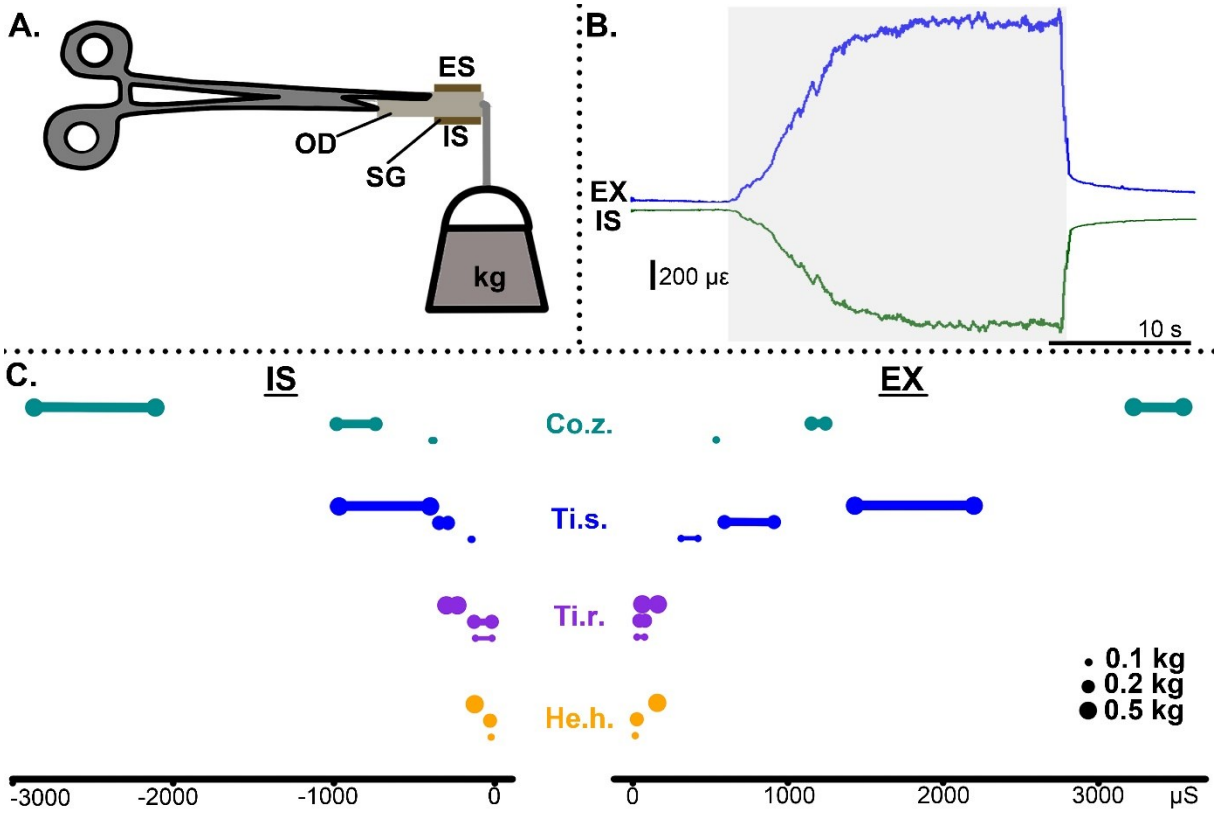

Fig. S1. 'Perpendicular Tensile' test experiment. A. Schematic representation of the 'Perpendicular Tensile' test experiment. B. Waveforms recorded from the external and internal sides of the osteoderms using single element gauges. The grey area highlights the time period during which the osteoderm was loaded. ES: external side of the dissected osteoderm. IS: internal side of the dissected osteoderm. OD: osteoderm. SG: single element gauge. C. Tensile and compressive strains recorded from a subsample of dissected ODs. Here, the OD was loaded perpendicular to its long axis using different weights (100, 200, 500g) and strains were recorded along that axis using single strain gauges placed on the external and internal sides of the OD. *Co.z.: Corucia zebrata. He.h.: Heloderma horridum. Ti.r.: Tiliqua rugosa. Ti.s.: Tiliqua scincoides.*

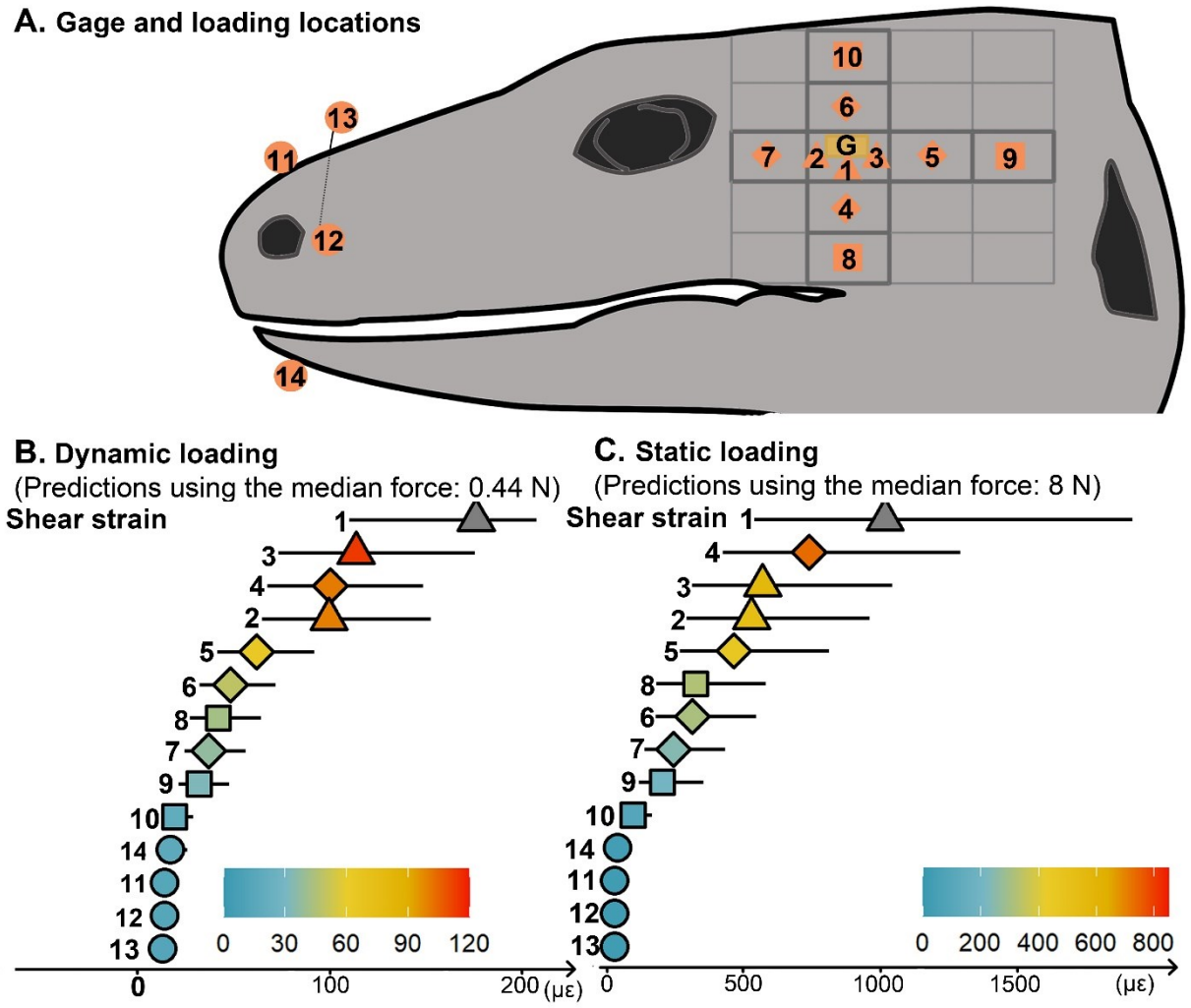

Fig. S2. Effect of the location of the loading on the shear strains predicted for the instrumented osteoderm. A. Location of the 14 different places where loading was applied. Locations are indicated by a triangle when force is applied directly on the instrumented osteoderm, a diamond when the force is applied on an osteoderm adjacent to the instrumented osteoderm, a square when it is applied to an osteoderm separated from the instrumented osteoderm by one osteoderm, and a circle when it is applied near the rostral end of the head. B. Shear strains predicted for each location by the Linear Mixed Model obtained using the 'dynamic' data. C. Shear strains predicted for each location by the Linear Mixed Model obtained using the 'static' data.

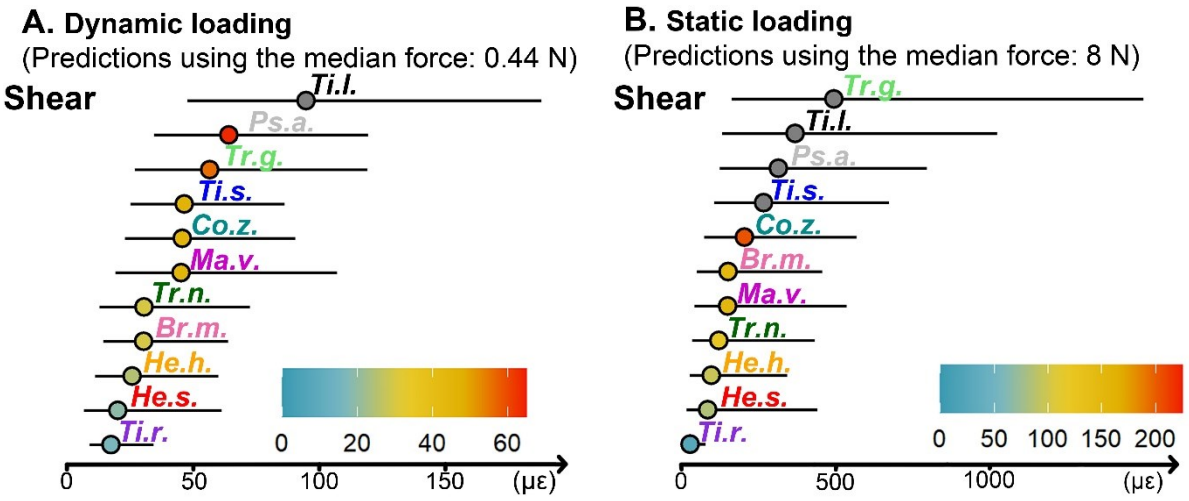

Fig. S3. *In-toto* interspecific differences in the stiffness of the skin system. The graphs show the shear strains predicted by the Linear Mixed Model for the instrumented osteoderm. All the locations were included in the model. *Br.m: Broadleysaurus major. Co.z.: Corucia zebrata. He.h.: Heloderma horridum. He.s.: Heloderma suspectum. Ma.v.: Matobosaurus validus. Ps.a.: Pseudopus apodus. Ti.r.: Tiliqua rugosa. Ti.s.: Tiliqua scincoides. Ti.l.*: *Timon lepidus. Tr.g.: Tribolonotus gracilis. Tr.n.: Tribolonotus novaeguineae.*

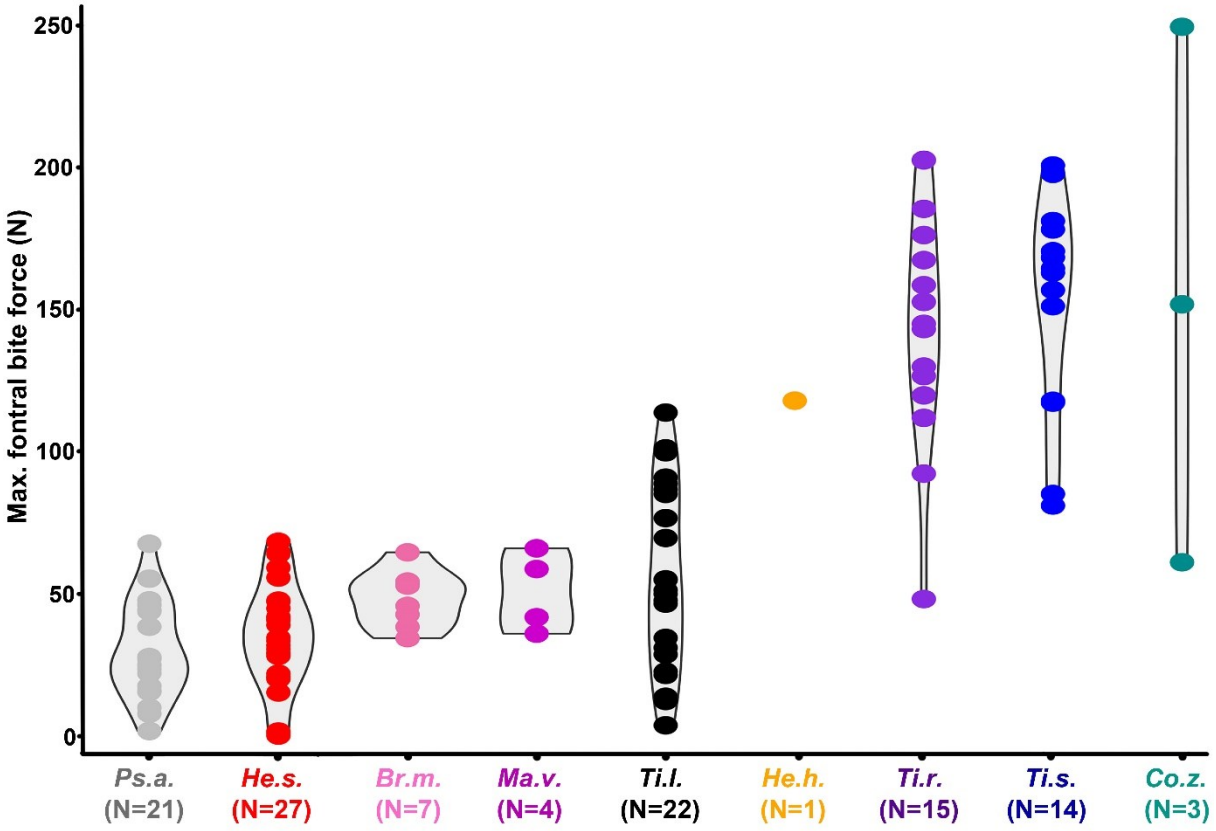

Fig. S4. Interspecific differences in the maximal bite force. Violin plots showing bite forces measured at the anterior end of the mouth for eight lizard species studied in this paper. Data are from a dataset from A. Herrel and were collected following the procedure described in Herrel *et al.* (1999). *Br.m: Broadleysaurus major. Co.z.: Corucia zebrata. He.s.: Heloderma suspectum. He.s.: Heloderma suspectum. Ma.v.: Matobosaurus validus. Ps.a.: Pseudopus apodus. Ti.r.: Tiliqua rugosa. Ti.s.: Tiliqua scincoides. Ti.l.*: *Timon lepidus.*

Table S1. Analysis of Deviance Table (Type III Wald chi-square tests). Loading Force was log-scaled. Signif. codes: 0 '***' 0.001 '**' 0.01 '*' 0.05 '.' 0.1 ' ' 1

Click here to download Table S1

Table S2. Shear (Log-transformed) strains predicted for a dynamic loading of 0.44 N and a static loading of 8 N.

Click here to download Table S2